LAWRENCE
LIVERMORE
NATIONAL
LABORATORY

UCRL-TR-227641

Final Report: Posttest Analysis of Omega II Optical Specimens

C. D. Newlander, J H Fisher

February 1, 2007

This work was performed under the auspices of the U.S. Department of Energy by University of California, Lawrence Livermore National Laboratory under Contract W-7405-Eng-48.

Final Report: Posttest Analysis of Omega II Optical Specimens

November 2006

Prepared for:
University of California
Lawrence Livermore National Laboratory
Attn: Kevin Fournier; L-473
PO Box 808
Livermore, CA 94551
Subcontract Number B560878

Prepared by:
Mr. C David Newlander
Dr. Jonathan H. Fisher
GH Systems, Inc.
655 Discovery Drive, Suite 302
Huntsville, AL 35806

Table of Contents

Figures

Tables

Posttest Analysis of Omega II Optical Specimens

29 September 2006-Draft
27 October 2006-Final

1.0 Background:

Preliminary posttest analyses have been completed on optical specimens exposed during the Omega II test series conducted on 14 July 2006. The Omega Facility, located at the Laboratory for Laser Energetics (LLE) at the University of Rochester was used to produce X-ray environments through the interaction of intense pulsed laser radiation upon germanium-loaded silica aerogels. The tests were performed under the direction of Dr Kevin Fournier/LLNL with the support of personnel from LLNL, SNL, and Alme & Associates. The optical specimen testing was supported by GH Systems through experiment design, pre- and posttest analyses, specimen acquisition, and overall technical experience. The test specimens were fabricated and characterized by Surface Optics Corporation (SOC), San Diego, CA and were simple protected gold coatings on silica substrates.

Six test specimens were exposed, five filtered with thin beryllium foil filters, and one unfiltered which was exposed directly to the raw environment. The experimental objectives were:

- Demonstrate that tests of optical specimens could be performed at the Omega facility.
- Evaluate the use and survivability of beryllium foil filters as a function of thickness.
- Obtain damage data on optical specimens which ranged from no damage to damage.
- Correlate existing thermal response models with the damage data.
- Evaluate the use of the direct raw environment upon the specimen response and the ability/desirability to conduct sensitive optical specimen tests using the raw environment.
- Initiate the development of a protocol for performing optical coatings/mirror tests.

This report documents the activities performed by GH Systems in evaluating and using the environments provided by LLNL, the PUFFTFT analyses performed using those environments, and the calculated results compared to the observed and measured posttest data.

2.0 Test Specimens:

Eight protected gold specimens were fabricated and characterized by SOC. The configuration was:

400 Å SiO_2/2000 Å Gold/0.2 cm SiO_2 Substrate

SOC measured the reflectivity of each specimen from 200 to 2000 nm. The spectrometer had a diameter of about 1 cm. Figure 1 shows the reflectance measured for the specimens over the range from 200 to 2000 nm. Also shown is a TFCALC calculation performed by GH Systems. Figure 2 shows a blow-up of the data and calculation from 200 to 500 nm. The correlation between the TFCALC

results and the measurements was poorer than expected. Discussions with SOC indicated that the silica coating may actually be closer to Si_2O_3 rather than SiO_2 as expected. SOC provided estimated refractive index properties that resulted in a reflectance curve as shown in the figure. This result appears to correlate less well than did the standard SiO_2 values. Additional analyses should be completed to find a set of materials and properties which match the pretest measurements accurately.

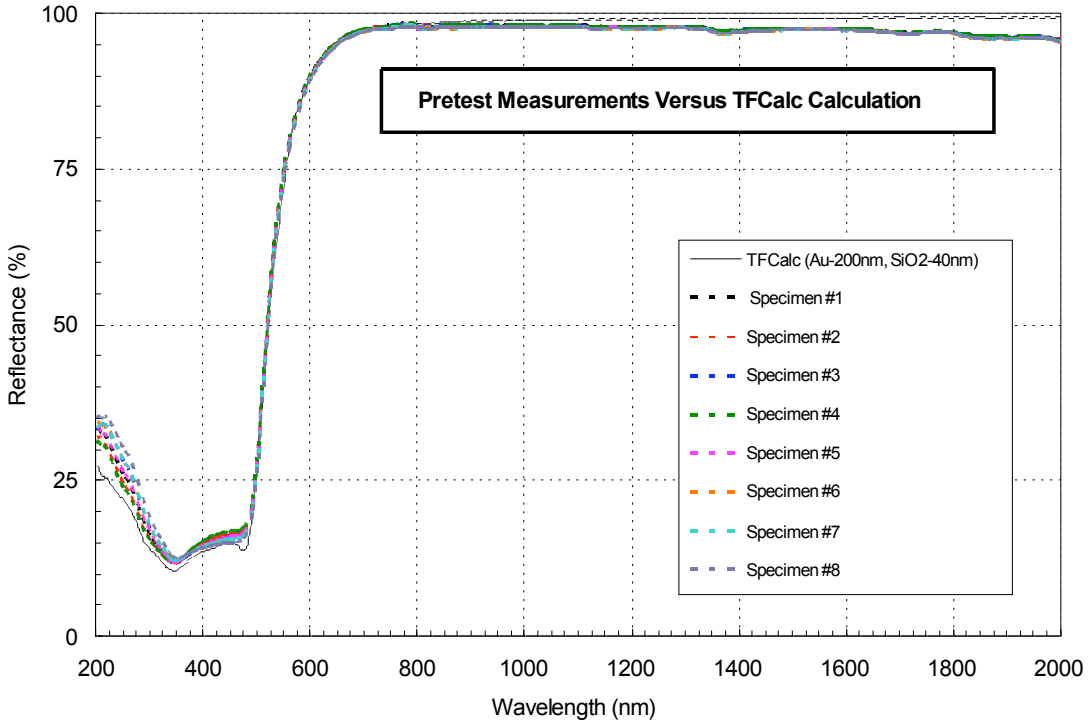

Figure 1. Pretest Reflectance Measurements Compared to TFCALC Calculations

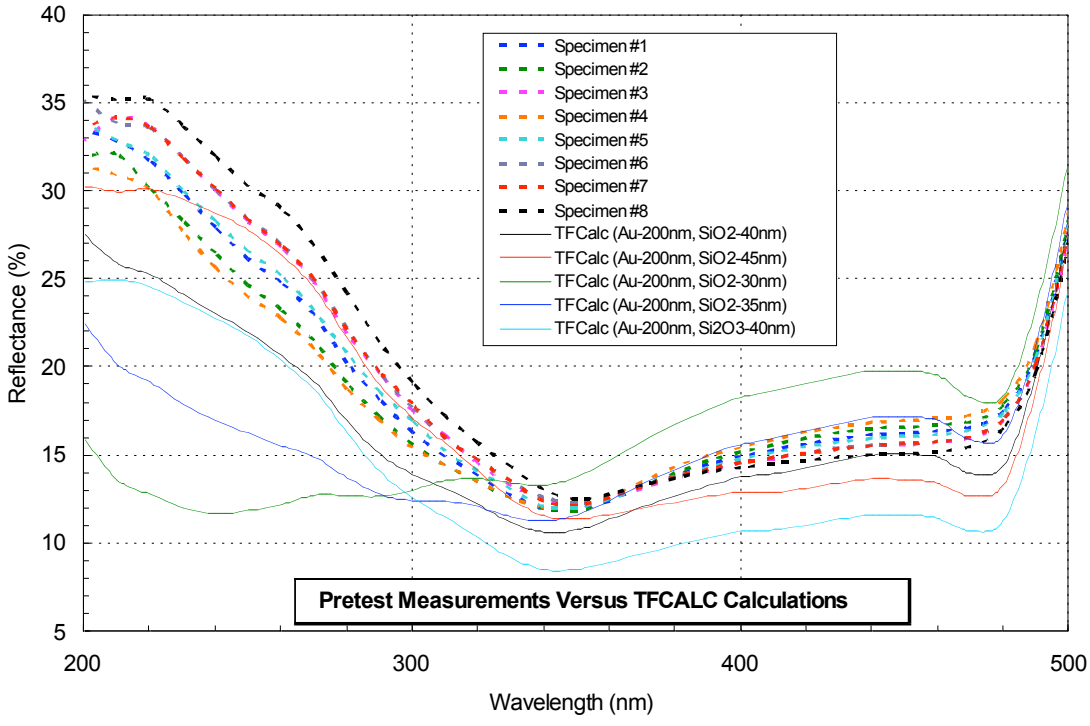

Figure 2. Measured and Calculated Reflectance Between 200 and 500 nm

The material used as the thin protective exterior layer can lead to significant uncertainties in the thermal and stress wave calculations and analyses. The thermal and stress models used for the exterior layer were for a high purity fused silica (amorphous SiO_2) which was used as the substrate material. (Note that crystalline SiO_2 is quartz which has a higher density [2.65 rather than 2.2 gm/cm^3] and can be used a piezoelectric stress gages). It was assumed that the properties for the bulk material would be appropriate for the thin film SiO_2 coating. This is just an assumption and contributes to the uncertainties in the analysis. If the material is actually SiO_x or Si_2O_3, then the material properties used are questionable and perhaps even the transmission through the "silica" into the gold reflective layer may have substantial calculational uncertainties. A major issue is with the Gruneisen parameter which strongly affects the generated stresses. Fused silica has a very low Gruneisen due its very low coefficient of thermal expansion (CTE – with units of cm/cm-^{o}C). No data have been found for Si_2O_3. This could result in considerable underprediction of the stresses actually generated in the silica coating layers. While there is always uncertainty in extrapolating properties from bulk materials to the thin coating materials, using a different material with no data tie points introduces even larger uncertainties.

Figure 3 shows a blow-up of the measured reflectance data between 600 and 2000 nm compared to the baseline TFCALC model results. Discussions with SOC indicate that the long wavelength discrepancy had to do with absolute measurement errors due the use of an integrating sphere. This results in a loss of several percent due to inefficiencies. SOC has received some new specular measurement standards and new equipment which will eliminate this problem in the future.

While the absolute measurement of the reflectance appears to have some issues, the relative measurements between the pretest and posttest specimens appears to adequate based upon the comparisons to be shown in Section 4.2. Measurements reported there for unexposed specimens correlate well between pre- and posttest measurements. In addition, the reflectance measurements appear to be consistent with the damage shown in the photomicrographs.

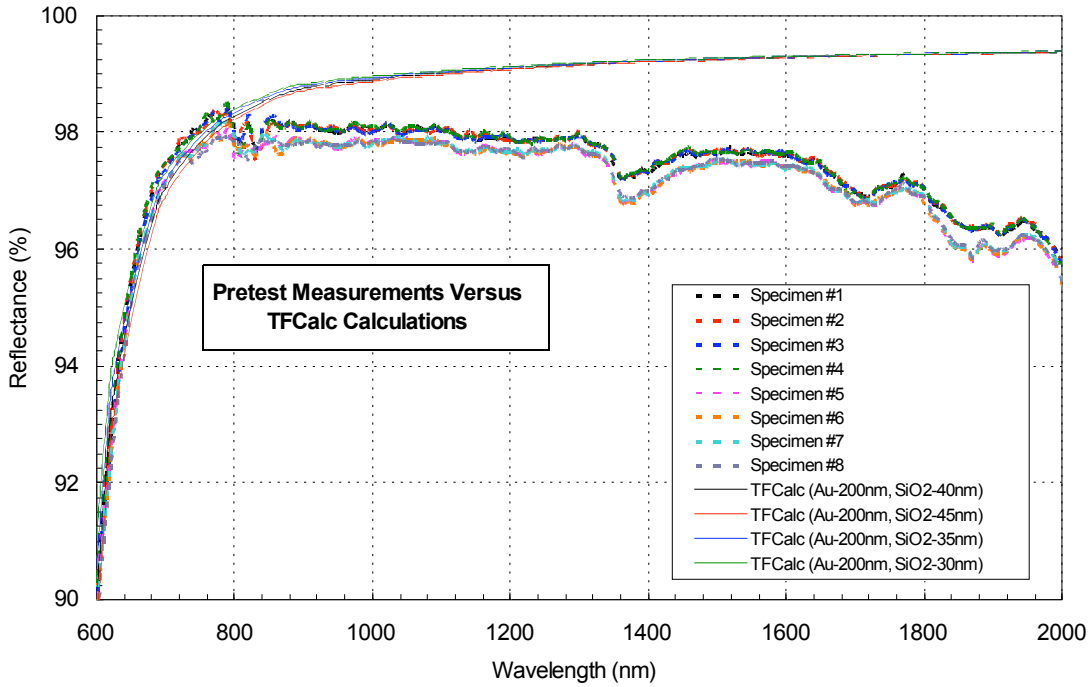

Figure 3. Measured and Calculated Reflectance Between 600 and 2000 nm

3.0 Environments:

3.1 Spectrum:

The LLNL team measured the spectra from each shot using different techniques and equipment (DANTE – X-ray diode array and HENWAY – crystal spectrometer) which were designed to determine the radiation distribution over a range of specific energies. The procedures used are described in detail in Reference 1. The spectral data were provided as energy-intensity pairs, and the results from all six shots are shown in Figure 4. These spectra were originally quite different in the range from 1 to 3.5 keV than those measured in the previous test series using a different type of equipment (DMX – X-ray diode array). This issue has since been resolved and was the result of different data reduction techniques. The spectra measured in OMEGA II are felt to be accurate. The spectra shown in Figure 4 were converted into energy bin – fluence pairs, normalized to 1 cal/cm^2, and used to in the posttest analyses.

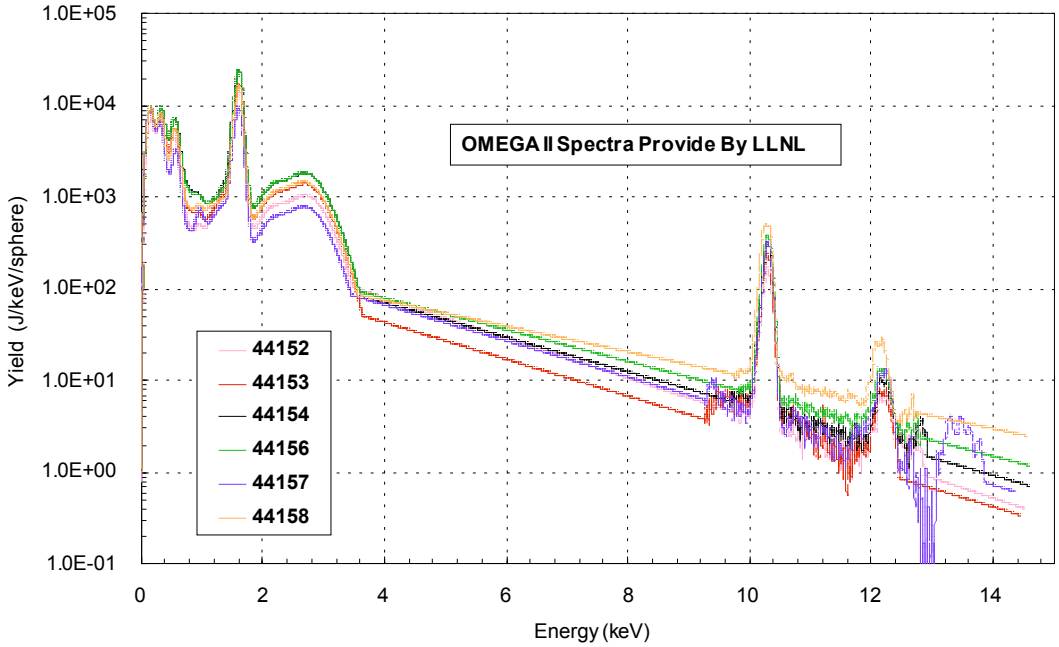

Figure 4. Measured X-ray Spectra Provided By LLNL

3.2 Fluence:

The fluence incident on the specimen cassette for the calculations was determined by integrating the LLNL-supplied spectra to determine the total yield and then scaling to account for the range from the source to the cassette front surface. There is some uncertainty due to uncertainties in the yield measurement in the region below about 3.5 keV. Comparisons of the two measurement types (DANTE and modified DMX) from the first series suggest fluence uncertainties on the order of ±11%. Table 1 lists the nominal fluences on the cassettes as calculated from the integration and scaling.

3.3 Flux-Time Pulses:

Two sets of flux-time profiles were provided; one set by LLNL which was supposed to be most consistent with the higher energy (9 to 15 keV) X-ray yields, and Sandia (SNL) measurements obtained using a PCD with an 8 mil Kapton filter which should be more representative of the softer, lower energy X-rays. There is considerable difference between the two sets of measurements as shown in Figure 5 for Shot 44152. Note that the LLNL data were provided as a graph in Reference 1, so only a fit to that data is shown in figure rather than a plot of the measured flux-time points. Also shown is a piece-wise linear fit to the SNL data which was used in the calculations. All of the data and fits have been normalized to a peak fluence of 1.0. Because the SNL data are appropriate for the lower energy X-rays, they were used in the thermal and stress wave analyses. Each SNL data set was fit with a series of linear segments for use in the analyses. These are shown in Appendix A.
There were two basic flux-time profiles generated during the test series; the first had an approximate full width at half maximum (FWHM) of 3 nsec (Shots 44152 and 44157) and the remainder had an approximate FWHM of 1 nsec (Shots 44153, 44154, 44156, and 44158).

Table 1. Fluences Incident Upon Cassette Front Surface Used in the Analyses

Shot	Yield (cal/ster)	Range (cm)	Fluence on Cassette (cal/cm^2)	Pretest Expected Fluence (cal/cm^2)
52	144.81	70.3	0.0293	0.0264
53	165.67	35.2	0.1337	0.1176
54	215.80	25.5	0.3319	0.2241
56	214.76	30.5	0.2309	0.1566
57	116.01	29.3	0.1351	0.1517
58	167.93	26.1	0.2465	0.2139

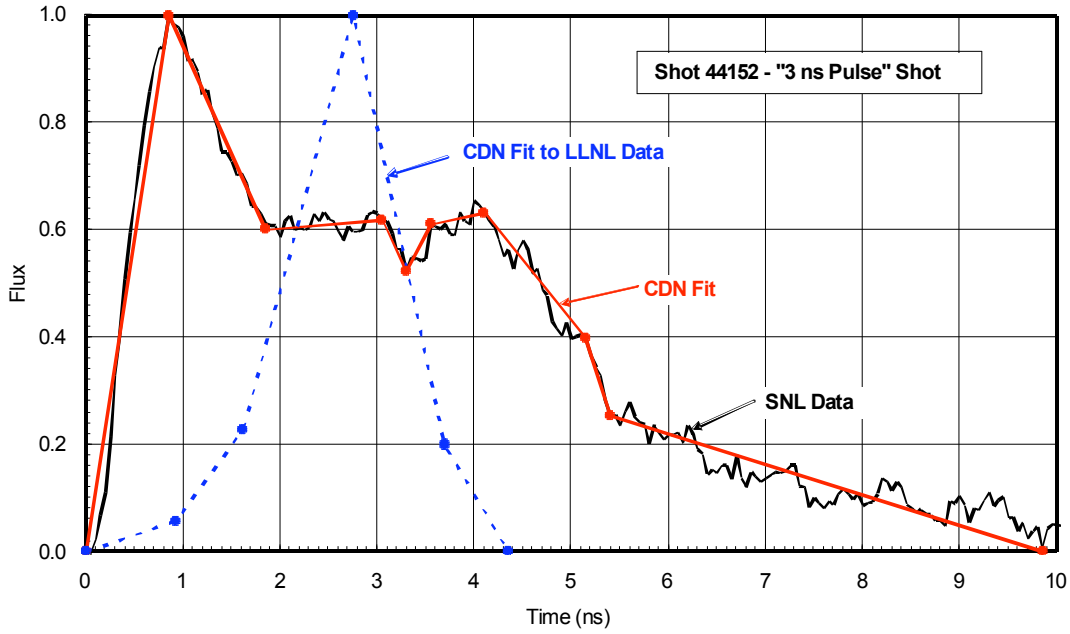

Figure 5. Comparison of LLNL and SNL Flux-Time Pulses for Shot 44152

4.0 Posttest Specimen Characterization

4.1 Posttest Photomicrographs:

Photographs were taken posttest during cassette disassembly at GH Systems. These show the cassette, specimens, and filters after X-ray exposure and testing and provide documentation of the disassembly procedure. Posttest photomicrographs of the specimens were taken at the ATK MR&TS Longmire Laboratory using an Olympus microscope with a Normarski set-up and an Olympus C-3030 camera. The photomicrographs have been examined and Table 2 indicates the condition of the coatings and substrates as determined by visual observations of the photos by

Newlander. Jonathon Fisher of GH Systems has indicated that some of the damage, such as scratches, may have actually occurred during the posttest reflectance measurements and are not the result of the radiation exposure. The posttest measurement techniques used in future test series will be modified to minimize such effects. Figures 6 through 12 show selected photomicrographs for the specimens. In summary, the photomicrographs show complete removal of the silica coating on Shot 52 (the only unfiltered shot), silica removal over several localized spots on Shot 56 (the specimen exposed to the highest fluence), and little to no damage on the remaining four specimens.

Table 2. Newlander Visual Observations of Posttest Photomicrographs

Shot	Specimen	Visual Observations
52	1	Outer layer(s) completely removed over entire exposure area. Based on reflectance data, the silica layer has been removed. Analyses and exposure area edge description suggest mechanical removal, not melt or vaporization. Gold layer appears to be intact
53	6	Only two photomicrographs available. One very small area shows removal of silica (folded back on itself indicating mechanical interface failure. Remaining silica and gold coatings remain intact and undamaged
54	5	Photomicrographs do not appear to be in focus. No damage to either coating is evident.
56	8	Silica coating removal at several areas. These areas appear to be a small percentage of the total exposed area. Close-ups of damaged area shows solid silica coating debris and folding of the layer at numerous locations. There may be several areas of cracking/splitting of the gold coating. These could be posttest scratches.
57	4	Beryllium filter fractured and failed on this shot. Specimens shows debris on the surface. There are also several long cracks/splits in the silica coating. The cause of the cracks/splits is unknown but could related to the debris impact or posttest scratches.
58	7	Photomicrographs do not appear to be focus. No damage to either coating is evident.

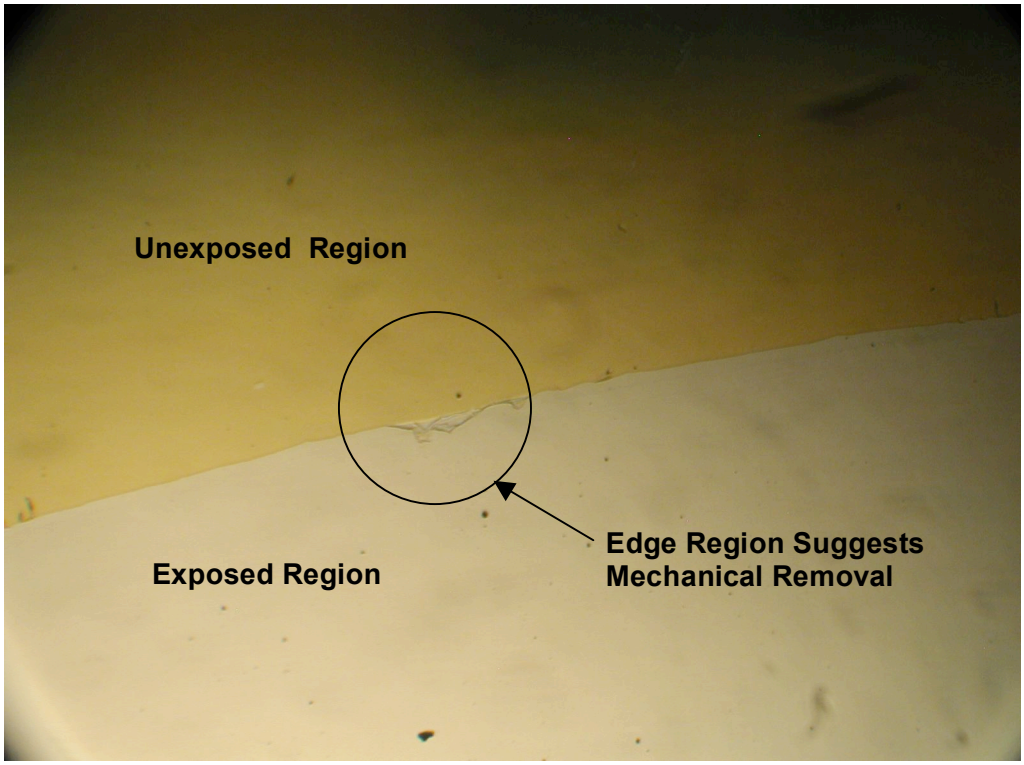

Figure 6. Photomicrograph of Specimen 1 (Shot 52). Silica Coating Layer Completely Removed Over Exposed Region.

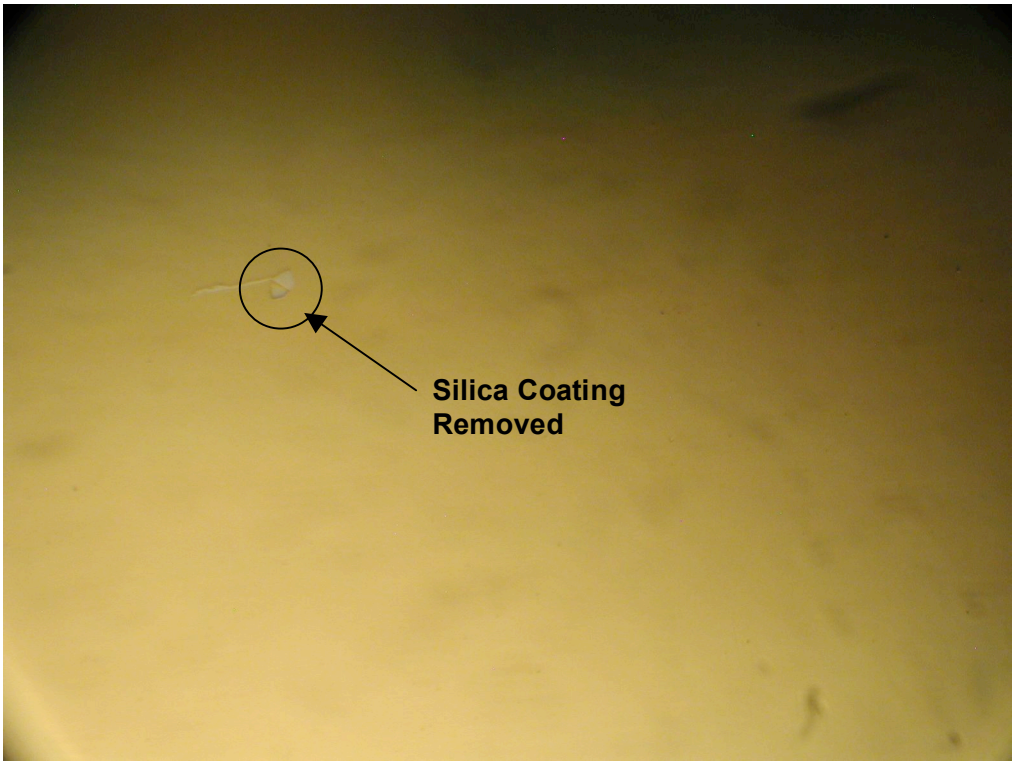

Figure 7. Photomicrograph of Specimen 6 (Shot 53). Silica Coating Layer Removed Over A Very Small Region.

Figure 8. Photomicrograph of Specimen 5 (Shot 54). No Apparent Damage to Either Coating.

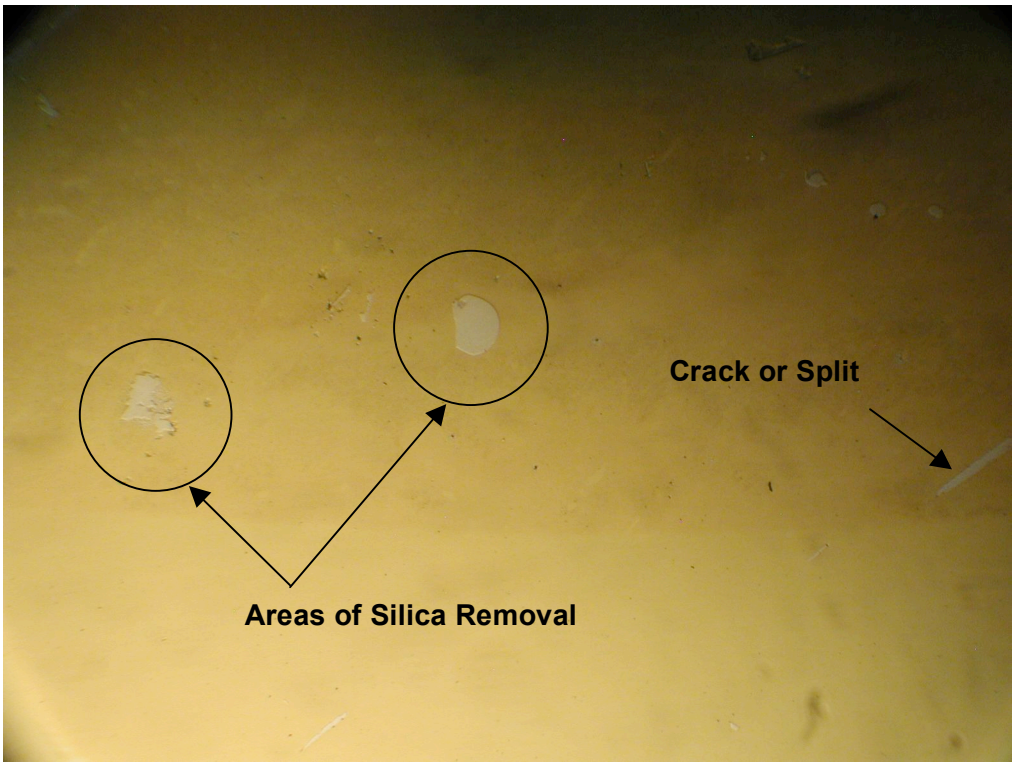

Figure 9. Photomicrograph of Specimen 8 (Shot 56). Complete Silica Coating Removal Over Several Areas. Several Cracks or Splits Observed in the Silica Layer.

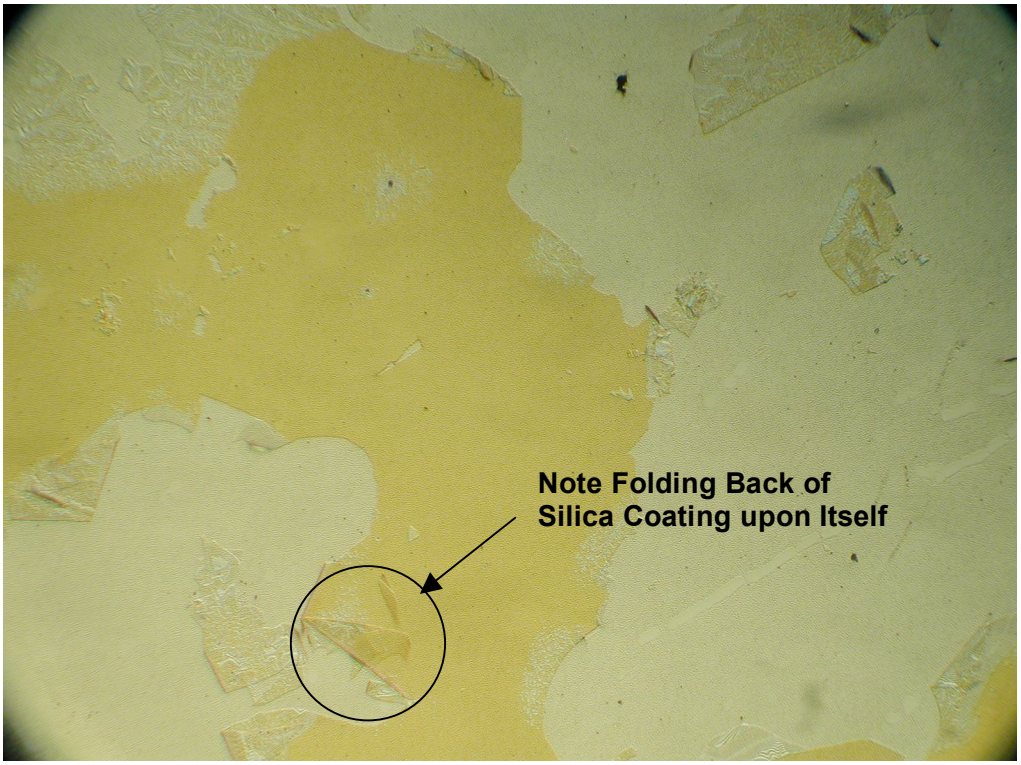

Figure 10. Close-Up of Specimen 8 (Shot 56) Showing Coating Removal And Fold-Over In Several Locations.

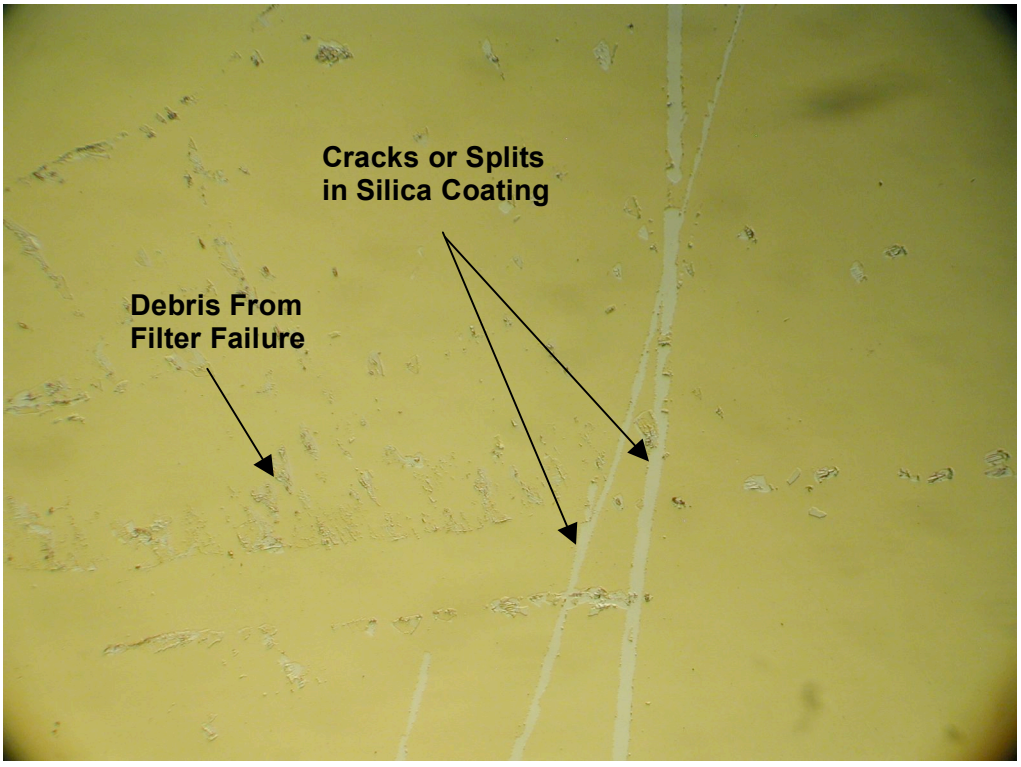

Figure 11. Photomicrograph of Specimen 4 (Shot 57) Showing Debris From Filter Failure and Cracks/Splits in Silica Coating.

Figure 12. Photomicrograph of Specimen 7 (Shot 58). No Apparent Damage to Either Coating.

4.2 Posttest Reflectance Measurements:

Surface Optics Corporation (SOC) measured the reflectance of the specimens after the radiation testing was performed. There were some problems with the absolute calibration of the reflectance measurements, but this was solved by also measuring the response of witness standards fabricated during the specimen coating run along with the tested specimens. Appendix B shows the measured pre- and posttest reflectance curves for the six tested specimens as well as the two spare, untested specimens (#2 and #3). Note that the posttest reflectance measurements were run from 300 to 3000 nm rather than down to 200 nm. Also show in the plots are TFCALC calculations for the baseline, untested configuration (400 Å SiO_2/2000 Å Gold/SiO_2 substrate) and a bare gold configuration without the SiO_2 coating. The loss of the silica coating increases the reflectance from 250 to 650 nm.

Figure 13 shows the measured pre- and posttest reflectance for Specimen #3 which was untested and therefore should show no effect of any X-ray exposure, but only the effects of handling and any laboratory testing. The pre- and posttest curves lie practically on top of each other. There is no degradation at any wavelength.

Figure 14 shows the results for Specimen #4 tested on Shot 57. This specimen was tested at the conditions designed to produce the lowest peak temperatures in any of the layers and the nominal fluence should produce peak temperatures below the melt temperatures of any of the layers. The filter for this specimen failed, and some debris on the surface was evident. In addition, several cracks or splits in the silica coating were seen in the photomicrographs. Again, the pre- and posttest curves lie practically on top of each other. There is no degradation in reflectance at any wavelength.

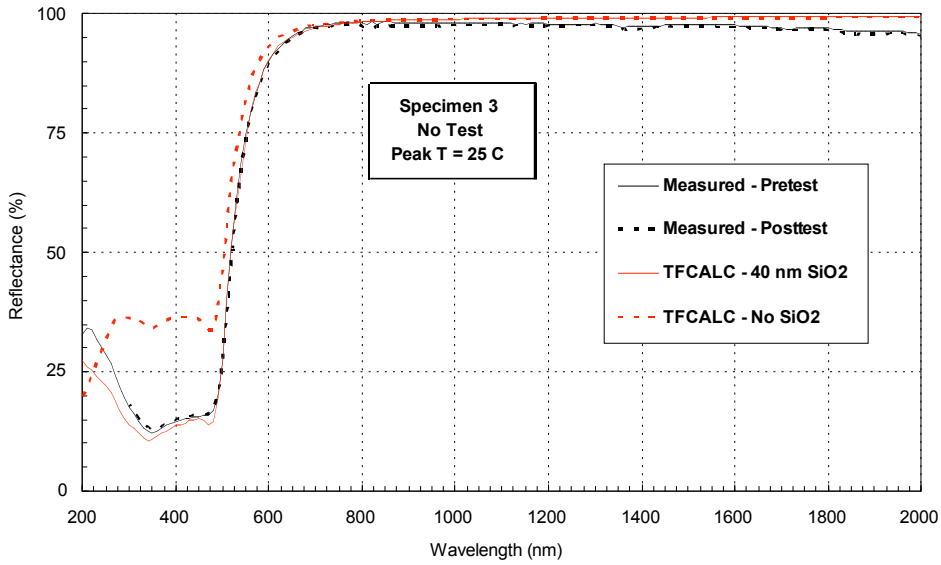

Figure 13. Pre- and Posttest Reflectance Measurements of Specimen #3 (Untested and Therefore No X-ray Effects)

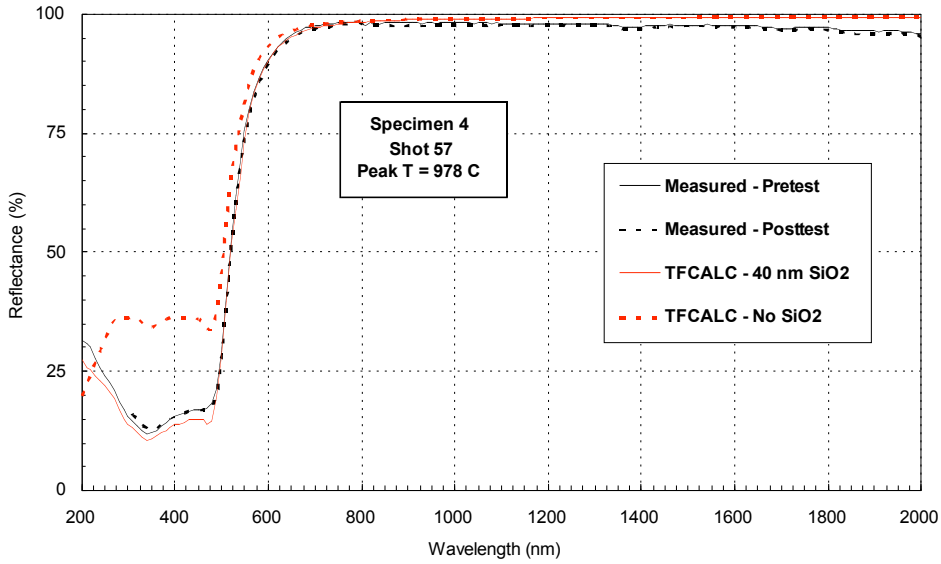

Figure 14. Pre- and Posttest Reflectance Measurements of Specimen #4 Tested on Shot 57. The Filter Failed On This Shot and Debris Was Detected On the Specimen Surface Along With Several Cracks/Splits in the Silica Coating Of Unknown Origin.

Figure 15 shows the results for Specimen #1 tested on Shot 52. The photomicrographs indicated that the entire silica protective coating layer had been removed by the X-ray exposure. The posttest measurements show enhanced reflectance in the UV and visible wavelengths. The TFCALC calculation without the silica overcoat matches the measured reflectance well and indicates that the gold layer was basically undamaged. There was no change in the reflectance above 800 nm which again suggests that the gold reflecting layer was undamaged by the X-ray exposure or the removal of the silica layer. This suggests that the gold layer probably did not melt.

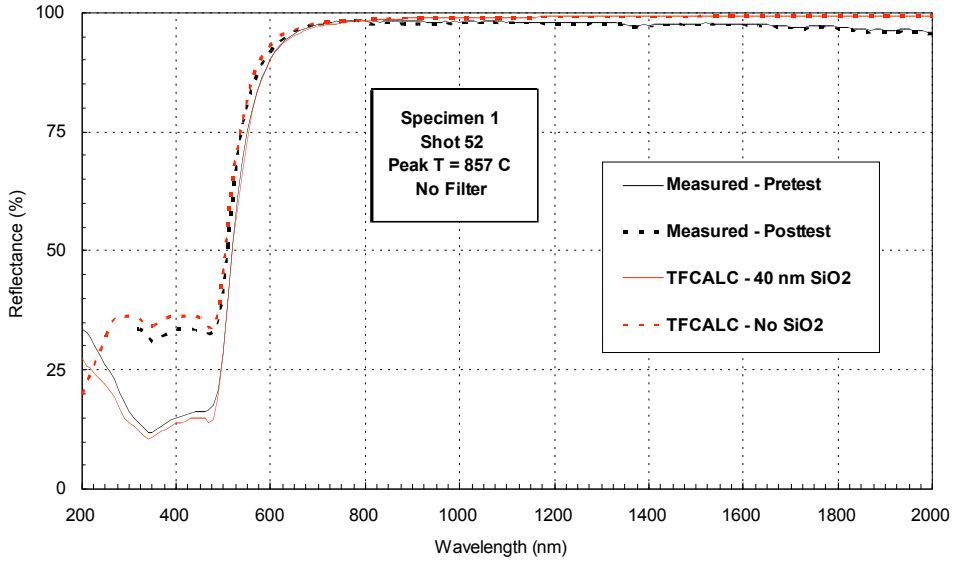

Figure 15. Pre- and Posttest Reflectance Measurements of Specimen #1 Tested on Shot 52. The Silica Coating Layer Was Completely Removed From the Exposed Region By Mechanical Response.

Figure 16 shows the results for Specimen #6 tested on Shot 56. The photomicrographs showed silica coating removal or several localized areas. The removal was mechanical as the silica coating could be seen folded back over itself in several locations. The reflectance curves show some reflectance increase in the UV which is probably attributable to the localized regions where the silica coating was removed. In addition there is some degradation in the wavelengths between about 550 and 700 nm that be due to some thermal damage to the gold reflecting layer. This is the only specimen that showed this level of degradation at this wavelength band and was the specimen tested at the highest fluence and gold peak temperatures.

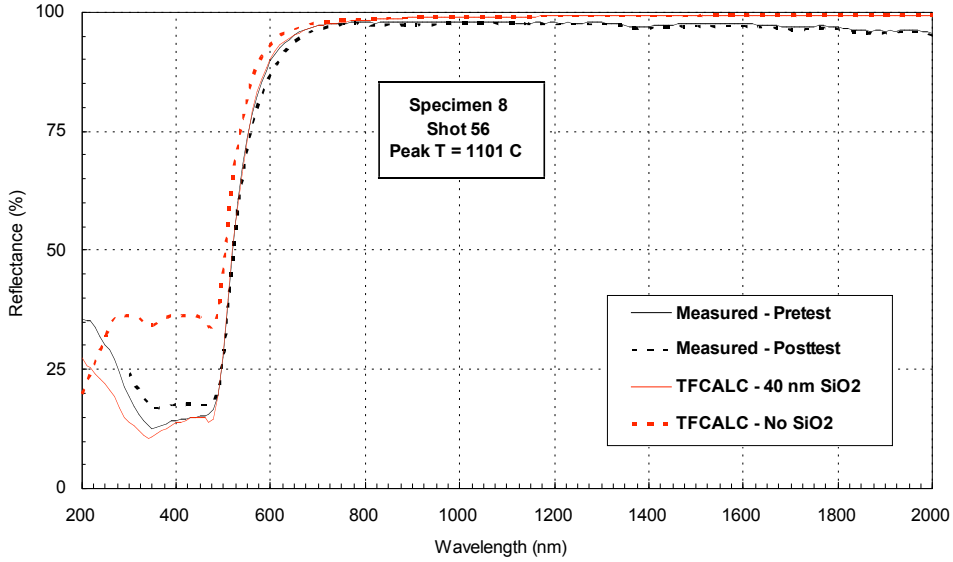

Figure 16. Pre- and Posttest Reflectance Measurements of Specimen #1 Tested on Shot 52. The Silica Coating Layer Was Completely Removed From the Exposed Region By Mechanical Response.

5.0 Posttest Calculations:

5.1 Transmission through Beryllium Foil Filters:

EPCAS radiation transport calculations were performed to transmit the raw spectra through the appropriate beryllium foil filter thicknesses. The properties of the beryllium foil material used in the analyses is shown in Table 3 and are based on elemental analysis performed on beryllium foils with similar levels of purity.

Table 3. Properties of Beryllium Foil Used in Analyses

Beryllium Foil (Density = 1.85 gm/cm^3)		
Element	Z	Weight Fraction
Beryllium	4	0.99682436
Nitrogen	7	0.00010000
Oxygen	8	0.00188064
Silicon	14	0.00031000
Copper	29	0.00084000
Molybdenum	42	0.00002000
Cadmium	48	0.00000500
Lead	82	0.00002000

Comparisons of the raw spectra compared with the filtered spectra are contained in Appendix C for each filtered shot. Table 4 shows the transmitted fluence fraction and the nominal fluence incident upon the specimen front surface for each shot.

Table 4. Fluences Transmitted Through Filters Used in the Analyses

Shot	Fluence on Filter (cal/cm^2)	Beryllium Filter Thickness (mils)	Transmitted Fluence Fraction	Fluence on Specimen (cal/cm^2)
52	0.0293	0	1.000	0.0293
53	0.1337	1	0.3383	0.0452
54	0.3319	2	0.2315	0.0768
56	0.2309	1	0.3565	0.0823
57	0.1351	1	0.3032	0.0410
58	0.2465	2	0.2429	0.0599

5.2 Initial Thermal Calculations:

PUFFTFT thermal calculations were performed using the baseline specimen design (400 Å SiO_2/2000 Å Gold/0.2 cm SiO_2 substrate). The calculations used identical thermal and mechanical properties for both the thin silica protective coating and the substrate which was known to be fused silica. The models used were developed by Newlander based on properties and data from Childs (Corning 7940) and other sources. Based on the discussion in Section 2, it is not clear what models should be used for the silica overcoat, and therefore there could be significant uncertainties in the results. Further sensitivity analyses should be performed.

The calculations used the spectra provided by LLNL and the piece-wise linear fits to the SNL-provided flux-time profiles. The fluences used were the nominal based upon the yield determined by the integration of the LLNL spectra, and ±11% to represent the extremes as suggested by LNLL after comparison of the DANTE and modified DMX results from the first test series.

Table 5 presents the calculated peak temperatures in the silica and gold coating layers for each of the calculations completed. The results are interesting. The lowest temperatures for the nominal conditions are for the longer, "3 nsec" pulses. Also, in general, the results are not very sensitive to the fluence. This is because the melt temperature for gold is 1064°C. Once the deposited dose reaches the incipient melt energy (and the melt temperature of 1064°C), any additional dose goes toward driving the material towards complete melt (through the heat of formation). The temperature remains constant at 1064°C until complete melt is reached, at which point the temperature will start to climb, but with the liquid heat capacity. This is shown in the gold temperature-enthalpy chart shown in Figure 17. Figure 18 shows the peak temperature envelopes for the unfiltered, "3 nsec" Shot 52 cases, and Figure 19 shows the envelopes for the filtered, "1 nsec" Shot 53 cases. All of the peak temperature envelopes are shown in Appendix D.

Table 5. Peak Temperatures From Initial Thermal Calculations

			Peak Temperature-°C (SiO_2/Gold)		
Shot	Pulse Width (ns)	Nominal Fluence	Nominal	-11%	+11%
52	3	0.0293	1045/1026	947/931	1107/1065
53	1	0.0452	1067/1065	1020/1020	1069/1065
54	1	0.0768	1085/1082	1077/1065	1096/1116
56	1	0.0823	1088/1101	1081/1076	1098/1124
57	3	0.0410	978/978	866/866	1065/1064
58	1	0.0599	1070/1065	1069/1065	1073/1065

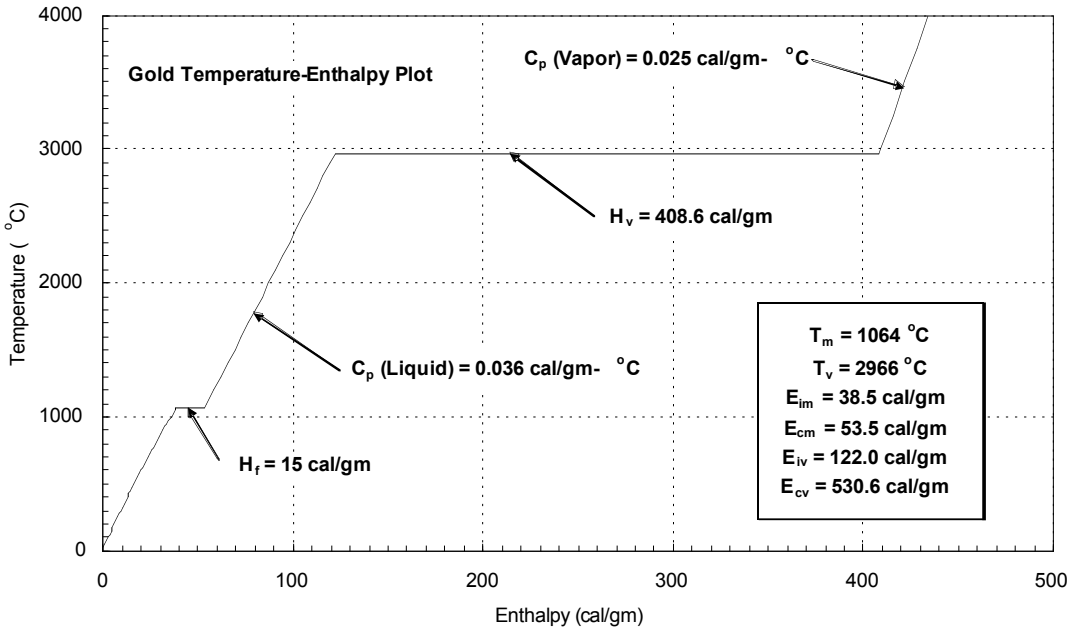

Figure 17. Gold Temperature-Enthalpy Plot

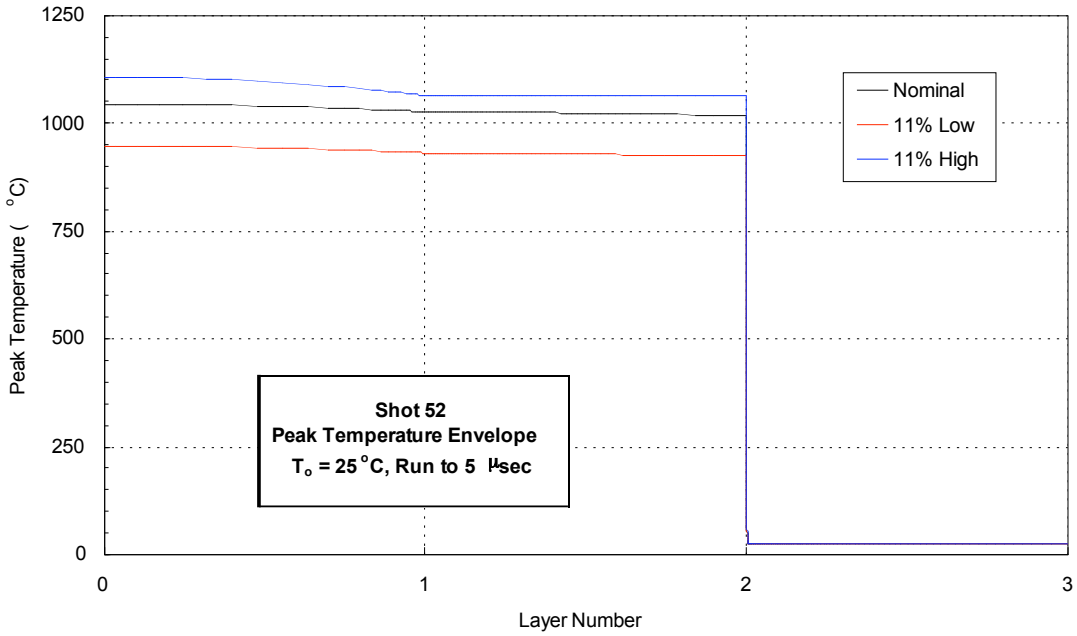

Figure 18. Peak Temperature Envelopes for Shot 52

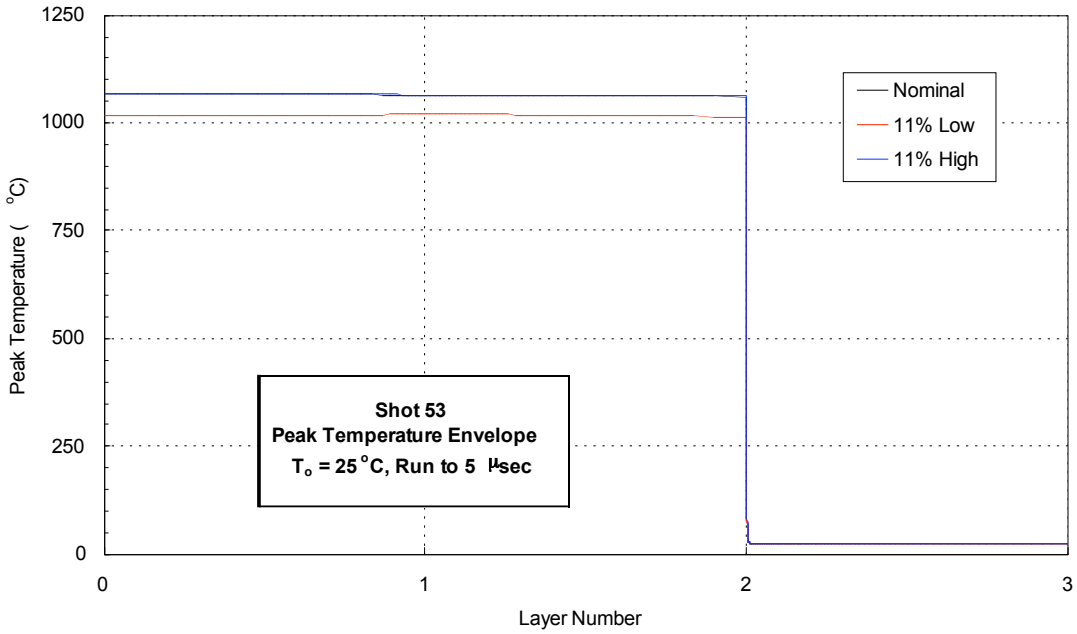

Figure 19. Peak Temperature Envelopes for Shot 53

5.3 Comparison between Analysis and Specimen Posttest Damage

It had been assumed, based on previous testing, that the failure mode of these specimens would be related to the melt of the gold layer. This appears to be wrong based on the results of the posttest photomicrographs and reflectance measurements. There appears to be no evidence of gold melt except with possibly Specimen #8 which showed some reflectance degradation in the 550 to 700 nm band. This is also the specimen that showed the highest calculated gold peak temperatures. The major damage shown in the specimens was the mechanical removal of all or part of the silica protective layer. Analyses were performed to evaluate the potential for these failures due to the thermomechanical response modes of lateral stresses (pop-off) and transverse (through-the-thickness) stress waves (spall, delamination, and detachment).

5.3.1 Lateral Stress Analyses:

Lateral stresses are generated by differences in the thermal expansion characteristics of adjacent material layers. If the generated lateral stresses are too large then the lateral (or shear stresses) can cause the layers to be separated and removed by “popping off”. PUFFTFT can be used to estimate these lateral stresses and analyses were performed to compare the calculated stresses for several of the shots. Three shots were selected: Shot 52 where the silica coating was completely removed, Shot 53 which showed no damage in either the photomicrographs or the reflectance measurements, and Shot 56 which had the highest specimen temperatures and yet only showed silica removal over several local regions.

Figure 20 shows the calculated lateral stresses for Shot 52 versus layer number at various times (the PUFFTFT code is currently not set up to generate peak lateral stress envelopes). The figure indicates that the peak stresses are generated near 5 nsec. The analysis indicates that the stress difference between the silica and gold layers is about 0.55 kbars. This is a substantial stress and may well have exceeded

the shear strength between the layers. However, the analysis also shows that the gold layer has yielded through the thickness. The gold was assumed to be annealed and have a yield strength of less that 0.02 kbars. The gold also shows reverse yield as the material cools at later times. The results are also predicated upon the properties of the silica protective coating which was assumed (for material property definition) to be fused silica with a yield strength of 15 kbars. However it is also assumed to have a very low CTE of 0.55 which will reduce the lateral stresses. It is also interesting to note that the fused silica substrate (which really is fused silica) induces large lateral stresses at the gold/substrate interface. However, no mechanical removal of the gold layer was observed. The interface strength between the gold and the substrate may be much larger than the strength between the two coating layers.

These results can be compared to the lateral stresses calculated for Shot 53 (shown in Figure 21) which showed no removal of the silica coating. Shot 53 was filtered and had a shorter FWHM. The calculated peak temperatures using the nominal fluences were higher than those calculated for Shot 52. Because Shot 53 was filtered, the lateral stresses in the silica protective layer are the result of the temperature being conducted from the gold layer rather than the direct deposition. However the lateral stresses calculated at the silica-gold interface are much higher in Shot 53 than in Shot 52. Figure 22 shows the results for Shot 56 – Specimen #8 which had the very highest calculated gold temperatures. The calculated interface lateral stresses are similar to those calculated for Shot 53. And yet Specimen #8 showed only silica coating removal over a limited region of the exposed specimen surface.

The lateral stress analyses suggest that the removal of the silica protective layer was not the result of excessive shear stresses unless there is a very large specimen-to-specimen variation. Because all of the specimens were processed and fabricated in the same manner and coated in one batch it is doubtful that these variations occur.

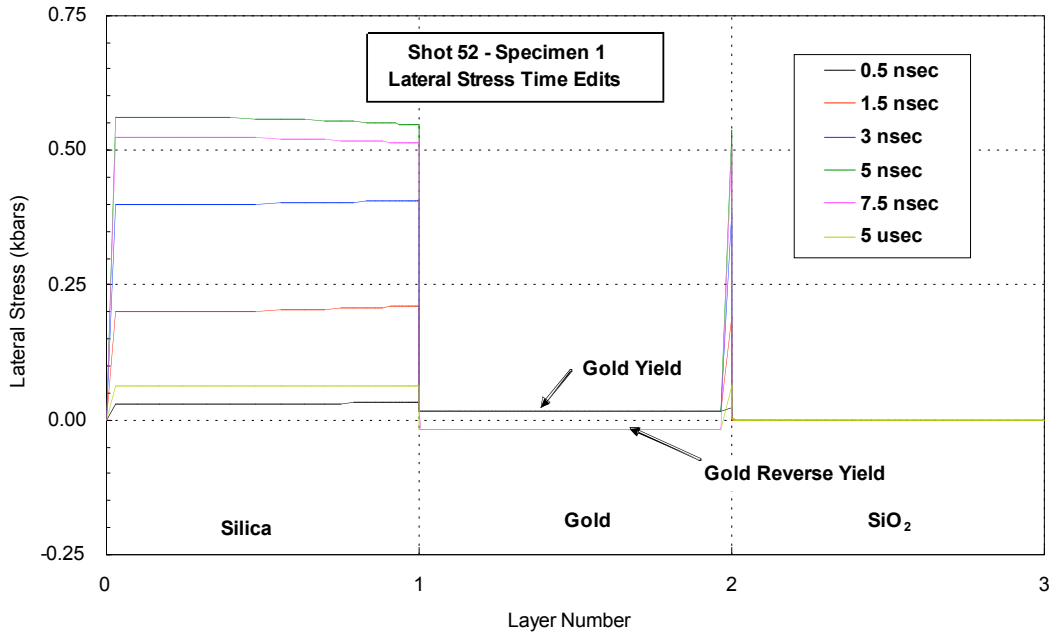

Figure 20. Lateral Stresses Calculated For Shot 52 – Specimen #1

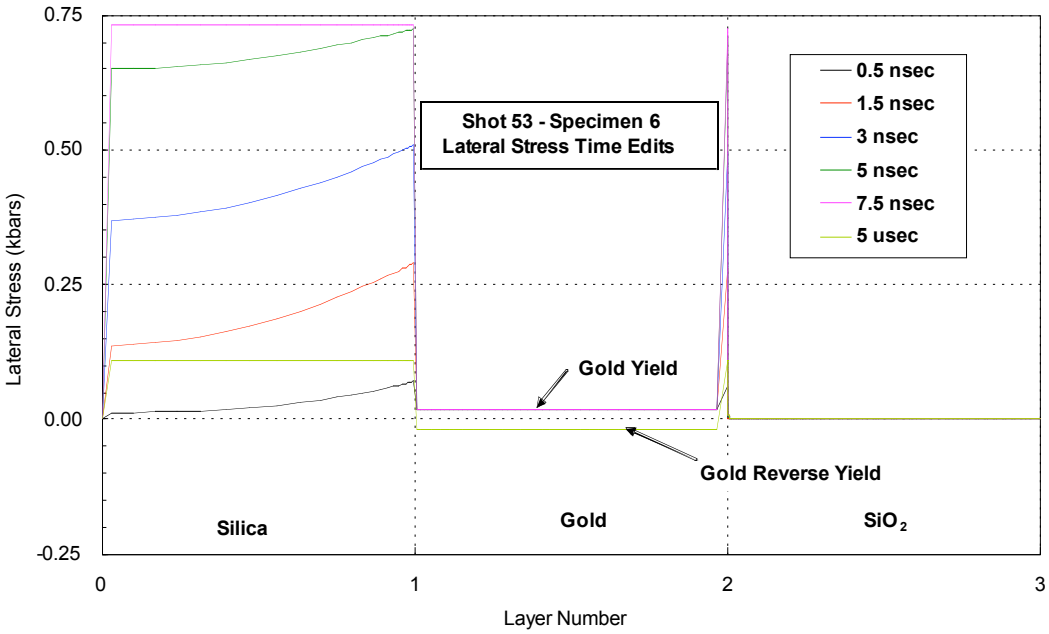

Figure 21. Lateral Stresses Calculated For Shot 53 – Specimen #6

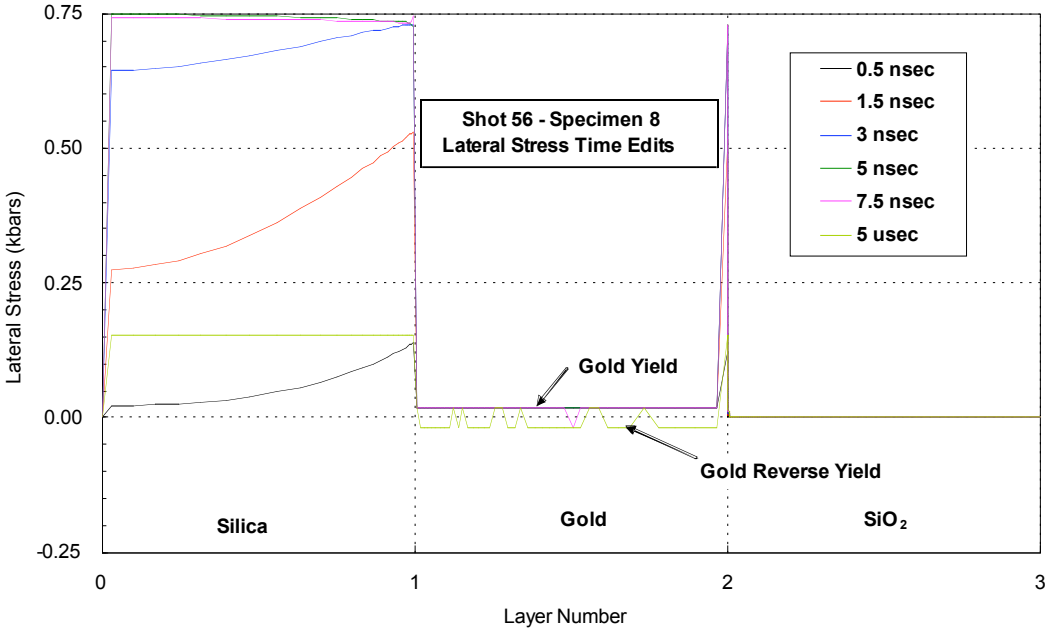

Figure 22. Lateral Stresses Calculated For Shot 56 – Specimen #8

5.3.2 Transverse Stress Analyses:

Calculations were performed to determine the transverse stress wave response of the specimens. It was felt that the damage seen in the Shot 52 which was unfiltered might be due to the stress waves generated in the silica coating due to the absorption of the low energy X-rays and UV. The calculations were very difficult to perform. Coupled thermal conduction - stress wave calculations were attempted using PUFFTFT but did not result in consistent, noise-free results due to limitations in the zoning and rezoning. Finally PUFF74 calculations were performed using hand zoning and no rezoning. These do not include the effects of thermal conduction, but

because of the thin layers, the stress wave transit time through the silica is very short (~0.01 nsec), and the conduction probably has a very low order effect on the generated peak stresses. Many stress wave transit times through the silica layer occur during the deposition process.

Figure 23 shows the calculated peak stress envelopes for Shots 52 and 57 run to 2 nsec. The silica coating was completely removed in Shot 52 and intact in Shot 57. There is some very early time noise in Shot 52 (the spike is actually calculated during the first hydrodynamic cycle and must be related to the zoning), but the trend indicates that the generated peak tensile stresses at the silica/gold interface could be nearly a factor of two larger in Shot 52 than in Shot 57. Spall or delamination of the silica layer may be the cause of the silica coating layer removal. However, there are large uncertainties in the material properties used and uncertainties inherent in the calculation itself.

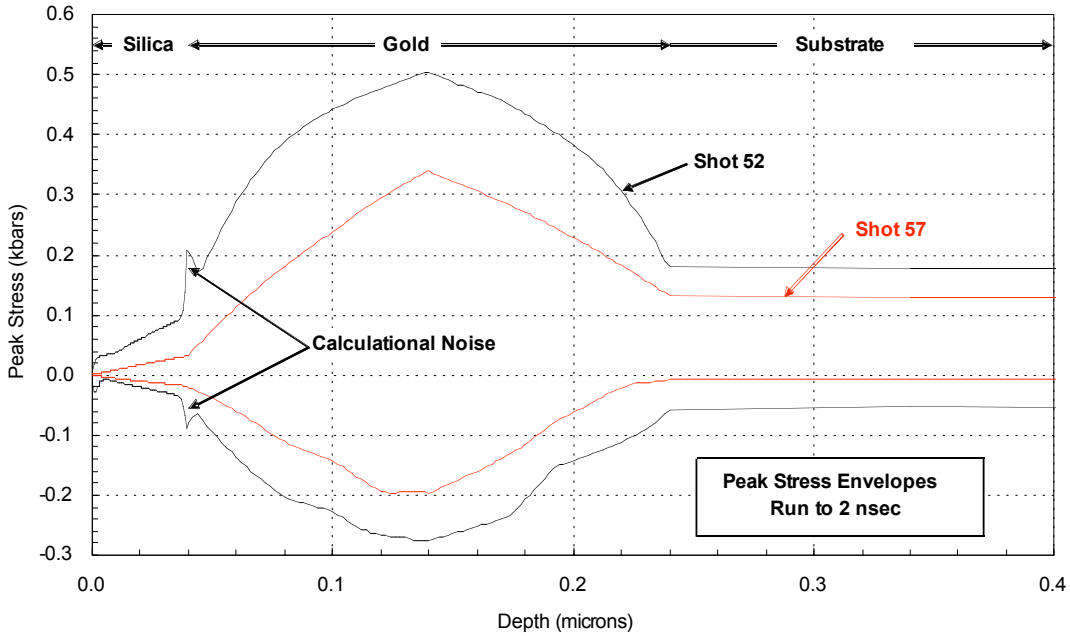

Figure 23. Peak Stress Envelopes Calculated for Shots 52 and 57

6.0 Summary and Recommendations

Optical specimen survivability testing was successfully completed at the OMEGA II facility. The posttest evaluation and analyses of the specimens indicate that both damaged and undamaged specimens were produced. The radiation environments were recorded and reduced such that reasonably accurate posttest analyses could be performed. Positive items associated with the effort include:

- The GH Systems effort provided characterized specimens and pretest analyses which allowed the testing to proceed on schedule for 14 July 2006 and within budget.
- The pretest analyses were accurate enough to select fluence levels (and source-target distances) such that both coating failures and undamaged specimens occurred near the levels predicted. Unfortunately the damage mode observed was different than that predicted.

- Posttest analyses have been performed to determine the response of the specimens to the radiation environments provided by LLNL.
- The final environments provided by LLNL and used by GH Systems for the posttest analyses appear to be relatively consistent although the nominal fluence may be somewhat high since there was little indication of gold melt, whereas the analyses suggest that there should be.
- The beryllium filters survived the radiation environments with the exception of Shot 57 where the filter failed and some debris was found on the specimen's surface.

There were a number of surprises and "lessons" learned that need to be addressed in order to improve the results of the next test series. These include:

- A test series dedicated to the performance of optical specimen testing would be highly desirable. This test series would be dedicated to producing the most repeatable radiation environment. This would allow the shot-to-shot uncertainties of the radiation source to be determined. The would mean holding the density of the aerogel target fixed and using consistent laser irradiation parameters.
- The measurements of the radiation environment need to be consistently made with appropriate equipment to provide accurate data on the spectrum, fluence, and pulse-widths for the energies of the most interest to the specimen testing.
- The areal uniformity of the radiation needs to quantified. The response of Shot 56 (Specimen #8) suggest that there may be "hot spots". The uniformity of the radiation environments on the specimen could also have been adversely affected by any epoxy on the back of the filters.
- Techniques need to be developed and demonstrated for determining the degradation in the optical performance of the specimens. These techniques need to be absolute in the sense that the posttest measurements can be directly compared to the pretest measurements without having to recalibrate the equipment.
- A technique to determine the thickness of material lost from the specimen front surface needs to be identified and used.
- The design of the baseline optical specimen for the next test series needs to be re-evaluated so that materials with known material properties are used and the damage mode is dependent upon the temperatures generated in the reflector layers. More complicated designs which may be damaged or fail from mechanical means can be tested in later test series.
- The test specimen cassette needs to be redesigned to eliminate the use of any adhesives and to eliminate any damage being induced in the specimen during assembly. The use of multiple exposures on larger samples should evaluated so that the response as a function of fluence or other conditions can be controlled without the issue of sample-to-sample variation. The use of a wedge-type filter with a known thickness gradient could be used to obtain different fluences across the specimen. This concept should be evaluated.

Given some additional funding, the following items should be completed to finalize the OMEGA II posttest effort:

- Measurements of the elemental composition of the specimen front surface, and the beryllium filter front and rear surfaces should be made. If significant epoxy is found on the rear surface of the filters, additional analyses need to be completed to evaluate the epoxy's effect upon the response of the specimen (energy deposition and the resulting temperature and stress response).
- The thickness of the material removed from each specimen front surface needs to be determined.
- Reflectance measures on small areas of the specimen surface should be completed to evaluate the response uniformity of the unexposed and exposed regions.
- Bi-Directional Reflectance Function (BDRF) measurements need to be investigated and performed on at least several selected specimens to evaluate its usefulness in defining the degradation as a function of test conditions.
- Additional TFCALC analyses should be performed to address the protective coating material and optical properties such that the calculated and pretest reflectance measurements correlate more closely.
- Material models should be evaluated and developed (along with uncertainties) for the silica coating material. Additional analyses using these models should be performed to try and understand the observed damage better.
- Analyses and investigations should be completed to determine the reason for the beryllium foil filter failure on Shot 57.
- It may be quite useful for GH Systems to analyze the aluminum stress wave measurements made by LLNL in an earlier test series. The correlation between the measured and calculated stress waves on well-known materials can provide an excellent method for evaluating environment and test uncertainties.

References

1. Fournier, Kevin B., et al, *Second Preliminary Report on X-ray Yields from OMEGA II Targets*, UCRL-TR-224095, Lawrence Livermore National Laboratory, Livermore, CA, 5 September 2006.

Appendix A

SNL Flux-Time Profiles and Piece-Wise Linear Fits

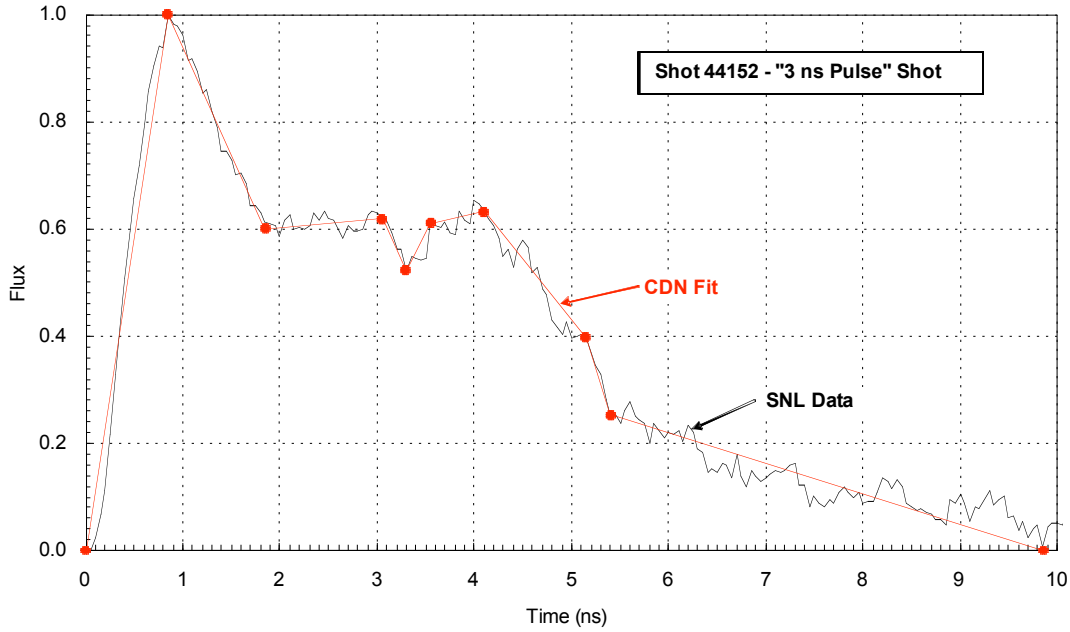

Figure A-1. Flux-Time Profile and Fit Used in Analysis for Shot 52

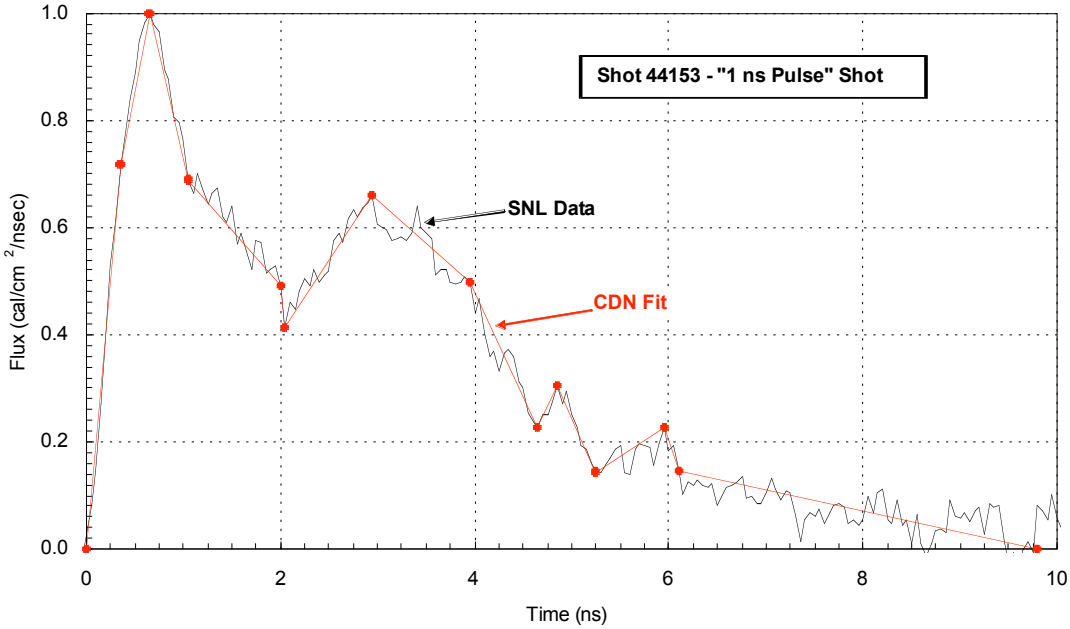

Figure A-2. Flux-Time Profile and Fit Used in Analysis for Shot 53

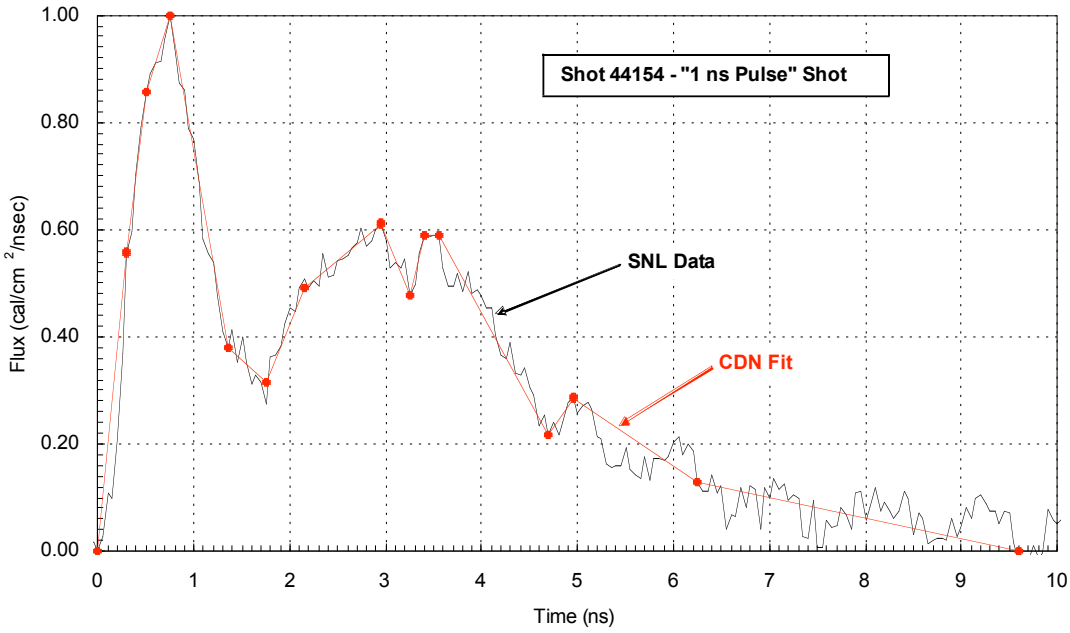

Figure A-3. Flux-Time Profile and Fit Used in Analysis for Shot 54

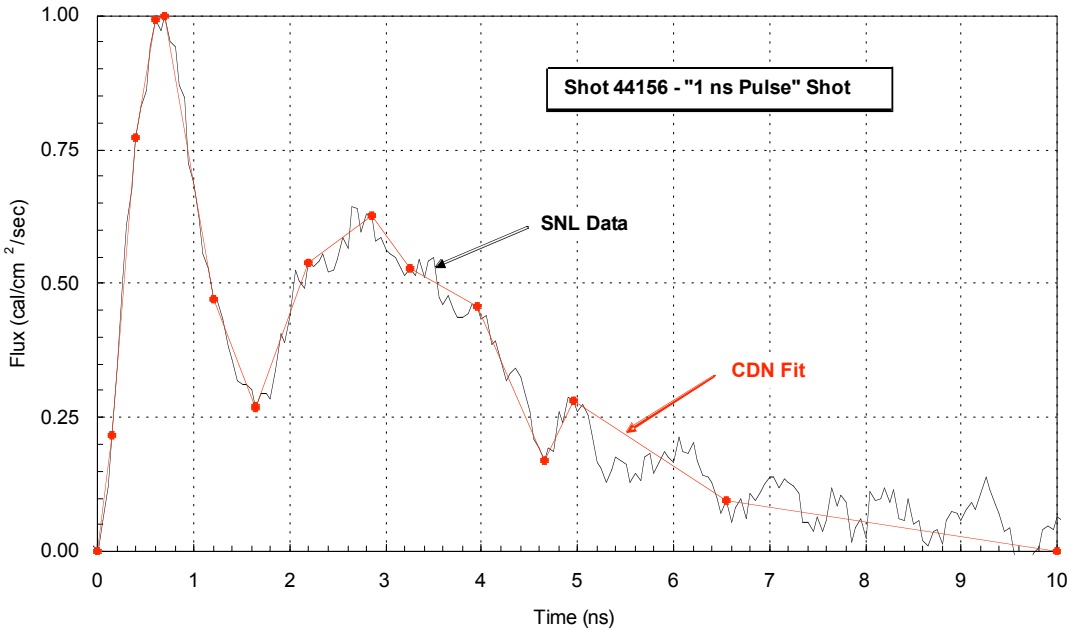

Figure A-4. Flux-Time Profile and Fit Used in Analysis for Shot 56

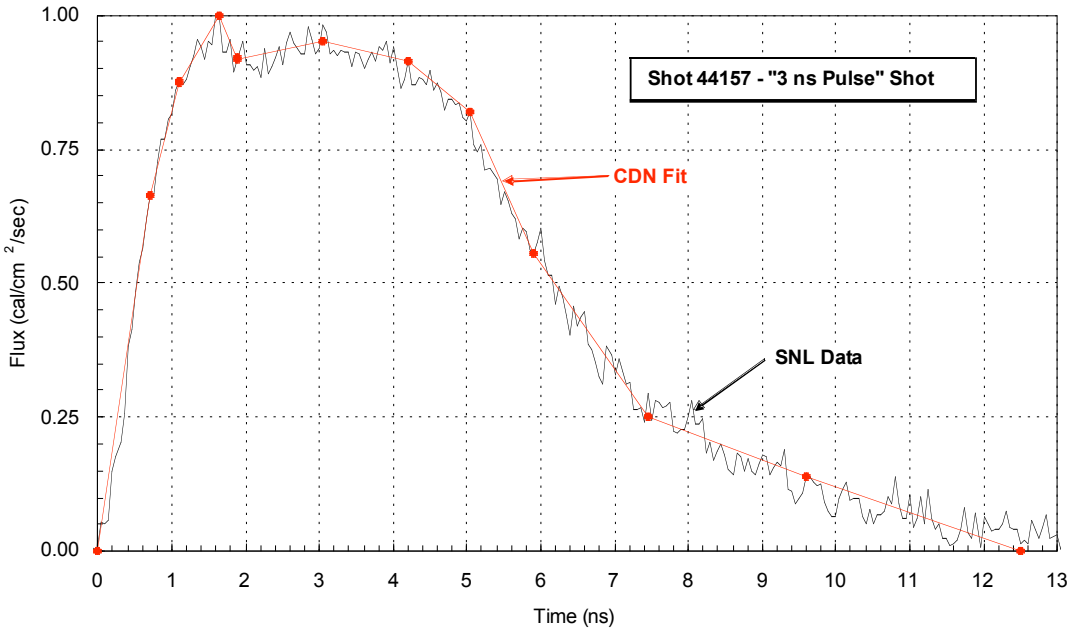

Figure A-5. Flux-Time Profile and Fit Used in Analysis for Shot 57

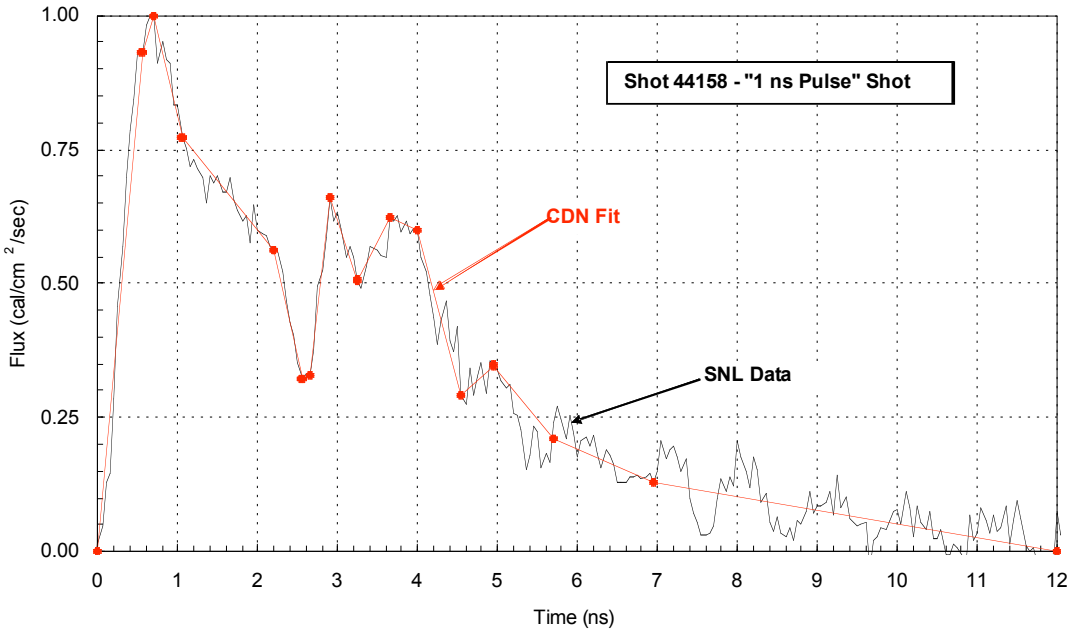

Figure A-6. Flux-Time Profile and Fit Used in Analysis for Shot 58

Appendix B

Pre- and Posttest Reflectance Measurements

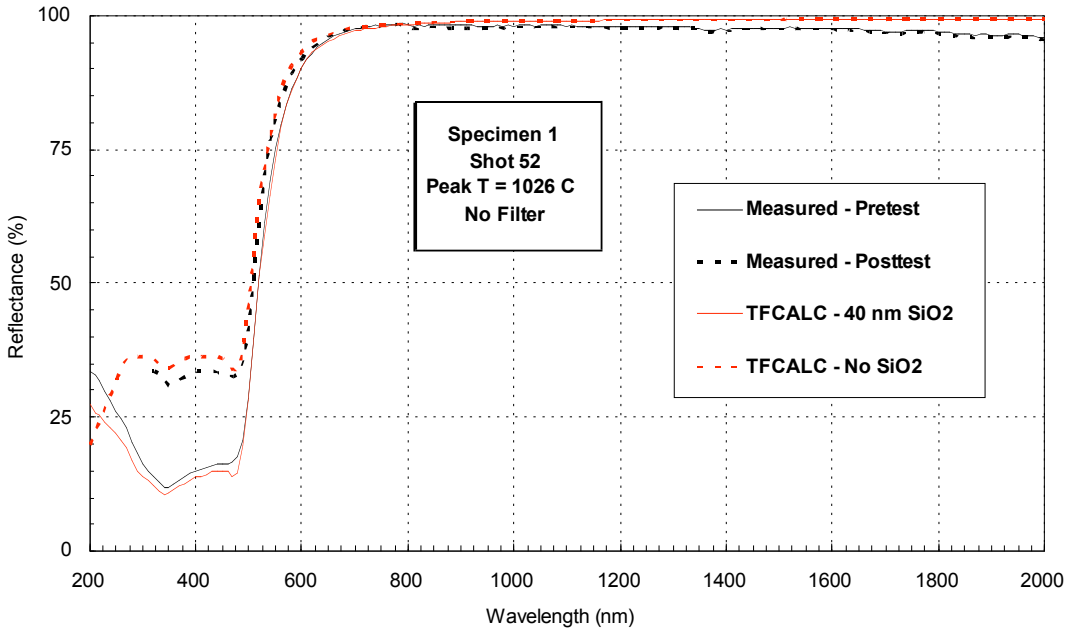

Figure B-1. Reflectance For Specimen 1 – Tested on Shot 52

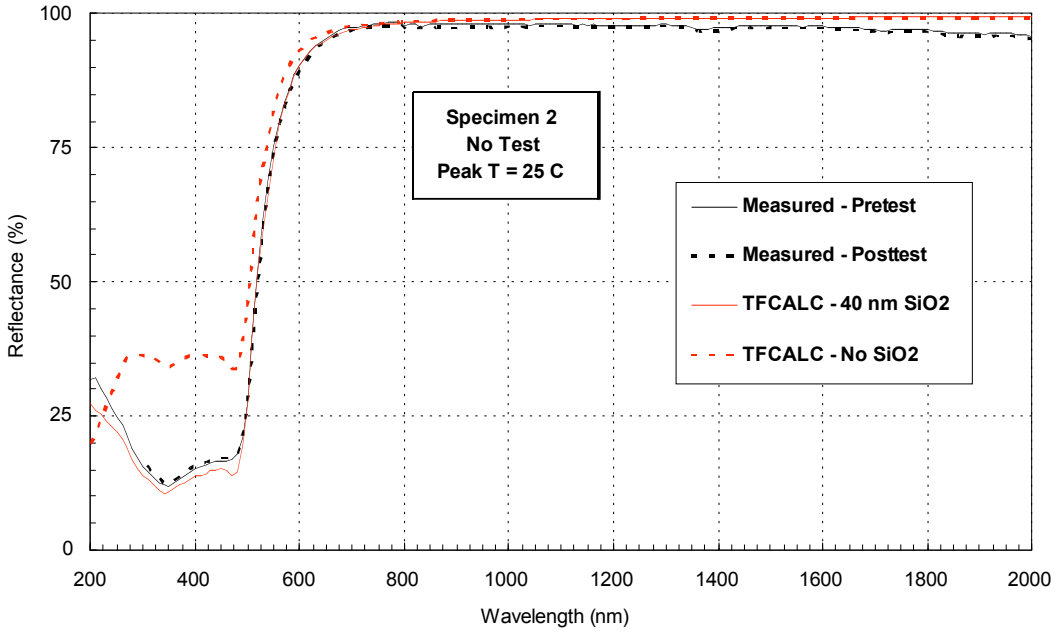

Figure B-2. Reflectance For Specimen 2 – Not Tested

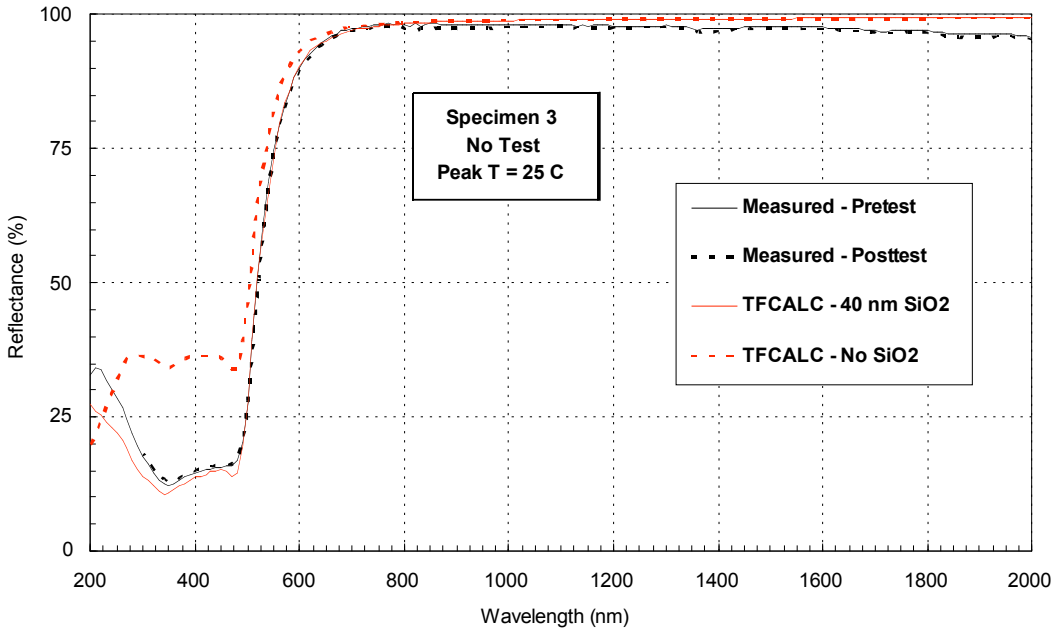

Figure B-3. Reflectance For Specimen 3 – Not Tested

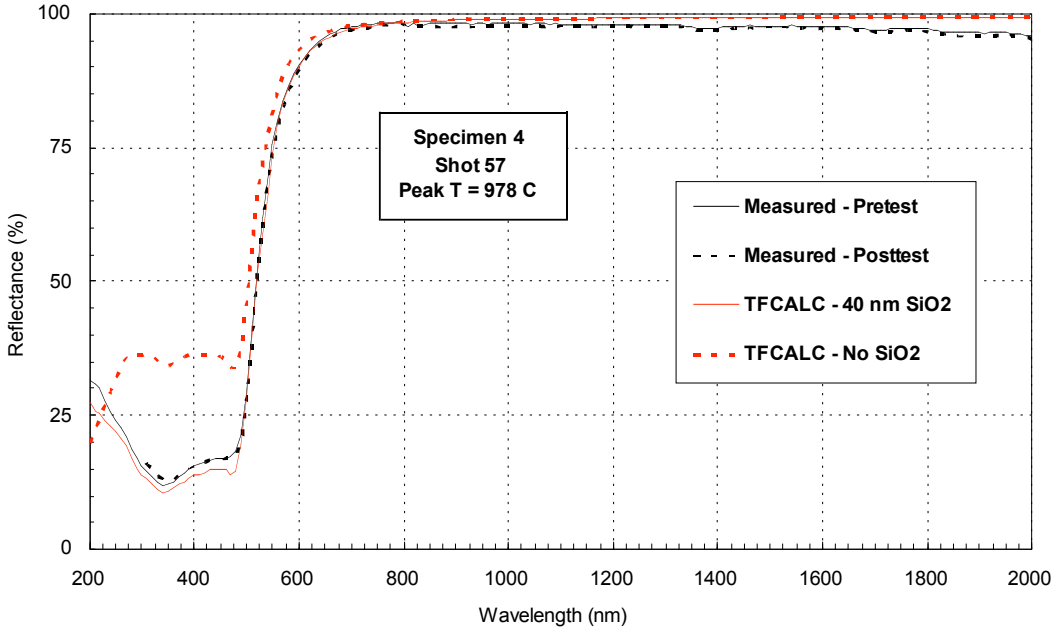

Figure B-4. Reflectance For Specimen 4 – Tested on Shot 57

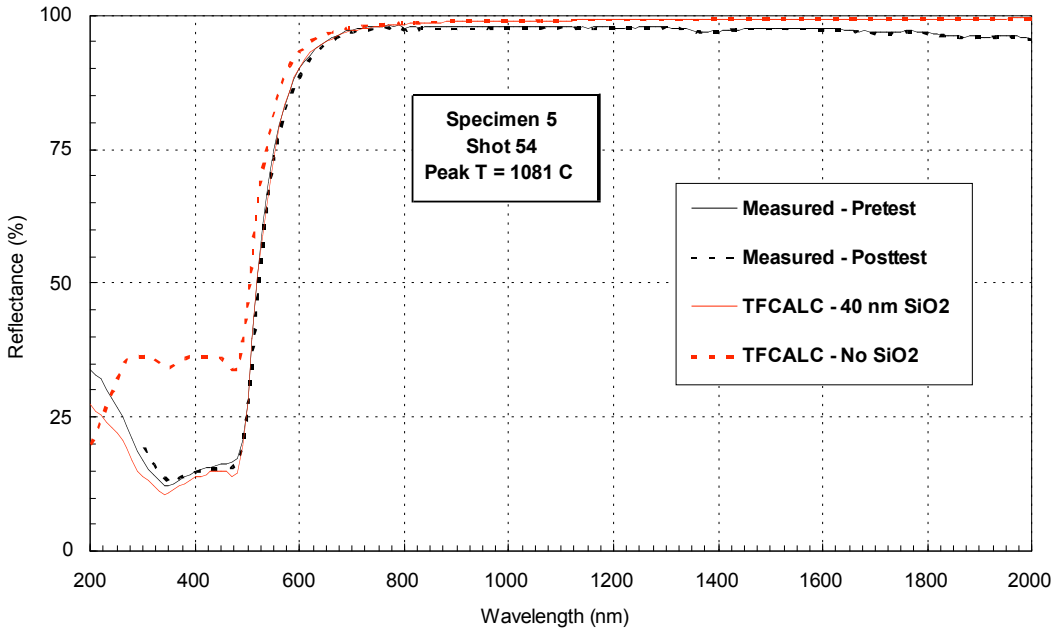

Figure B-5. Reflectance For Specimen 5 – Tested on Shot 54

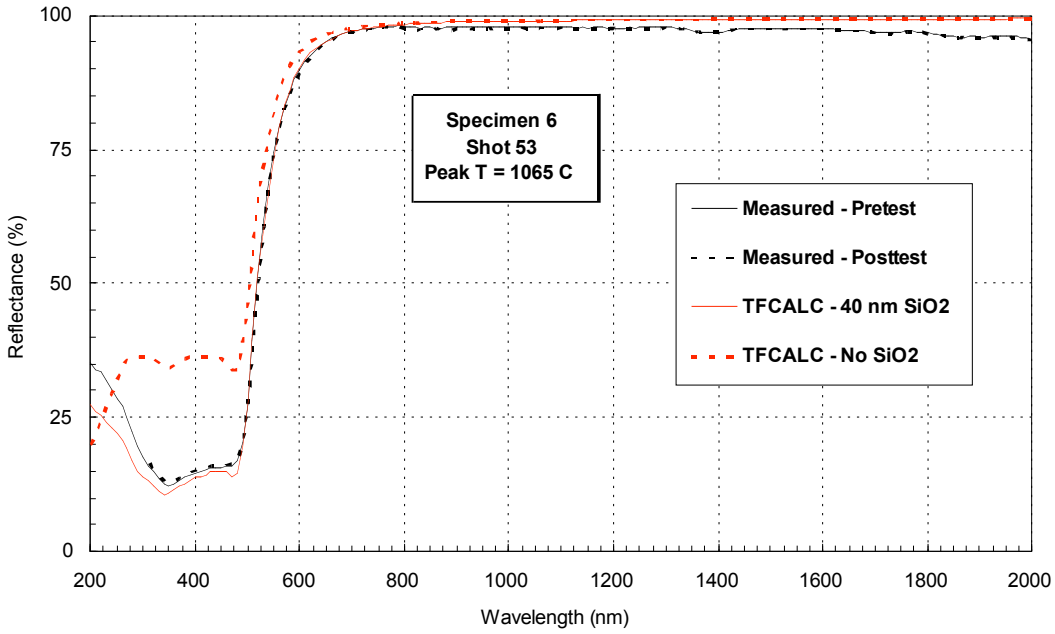

Figure B-6. Reflectance For Specimen 6 – Tested on Shot 53

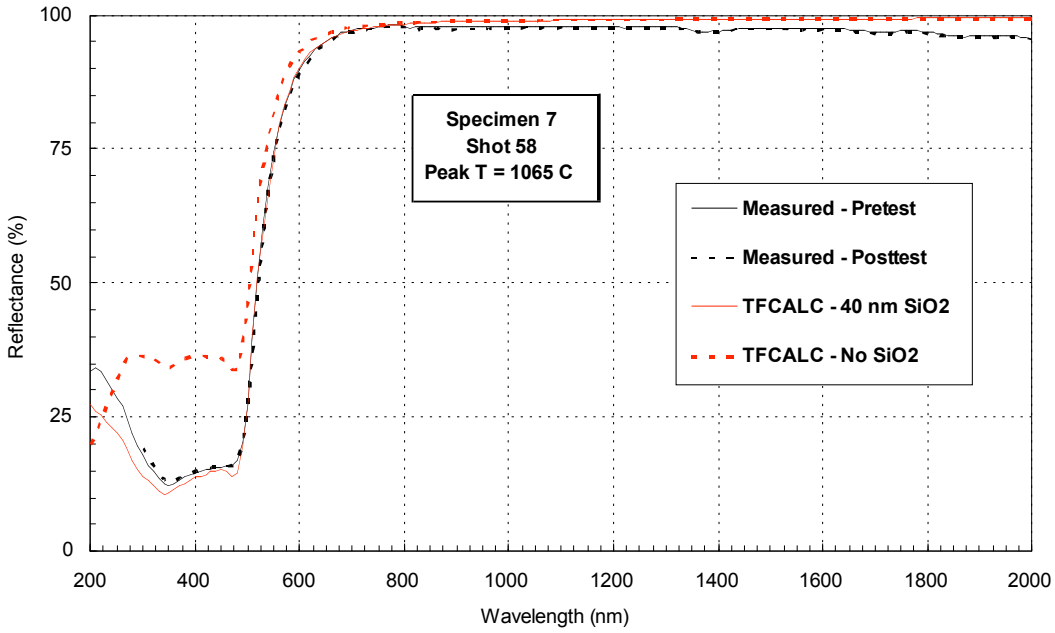

Figure B-7. Reflectance For Specimen 7 – Tested on Shot 58

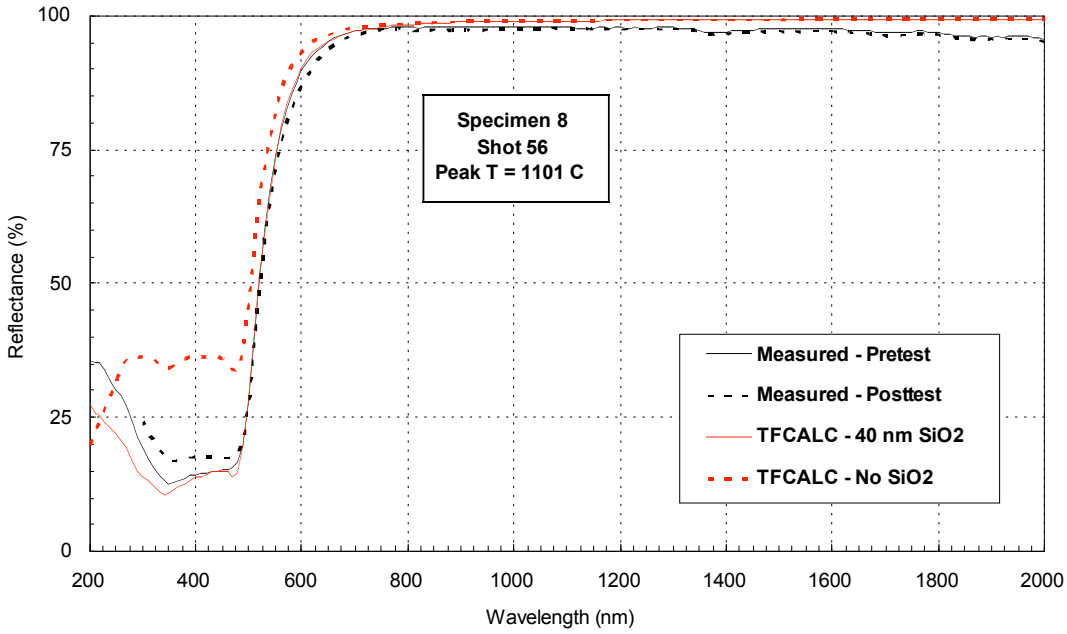

Figure B-8. Reflectance For Specimen 8 – Tested on Shot 56

Appendix C

Raw and Transmitted Spectra

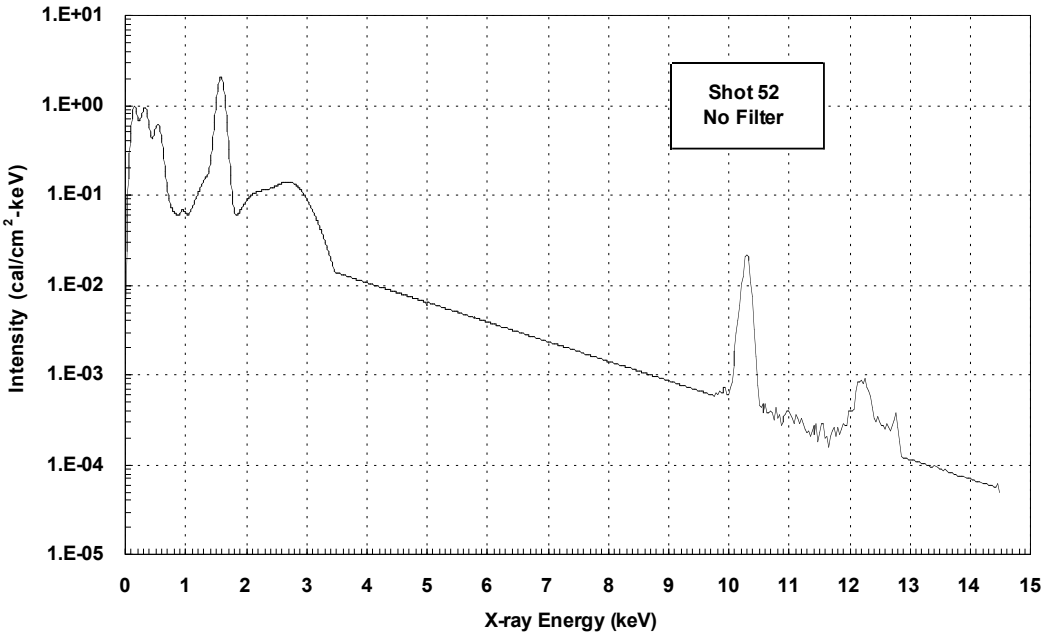

Figure C- 1. Raw Spectrum – Shot 52

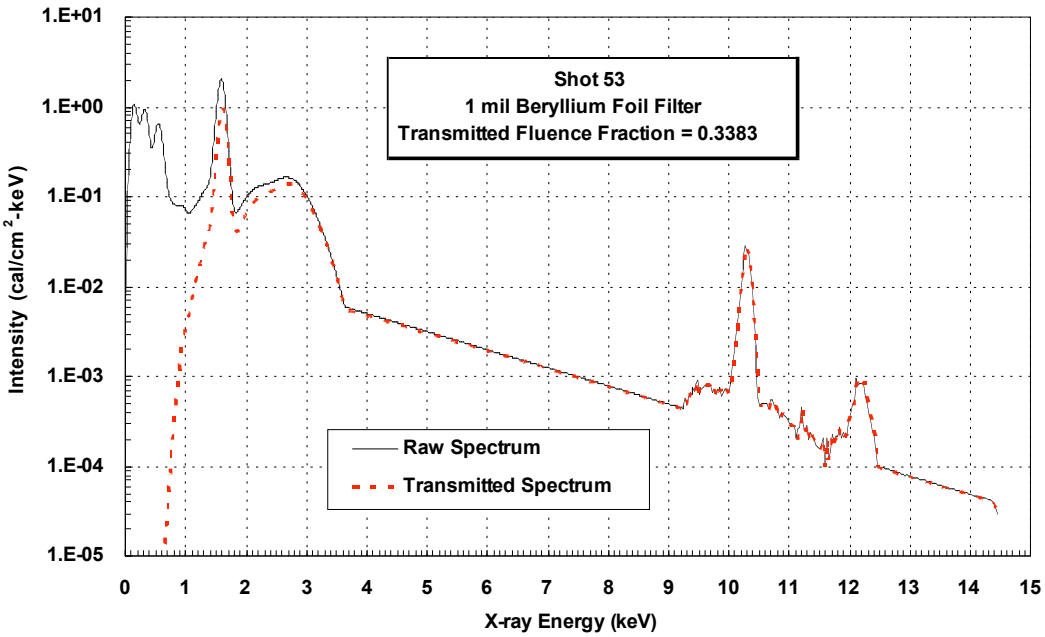

Figure C-2. Raw and Transmitted Spectra – Shot 53

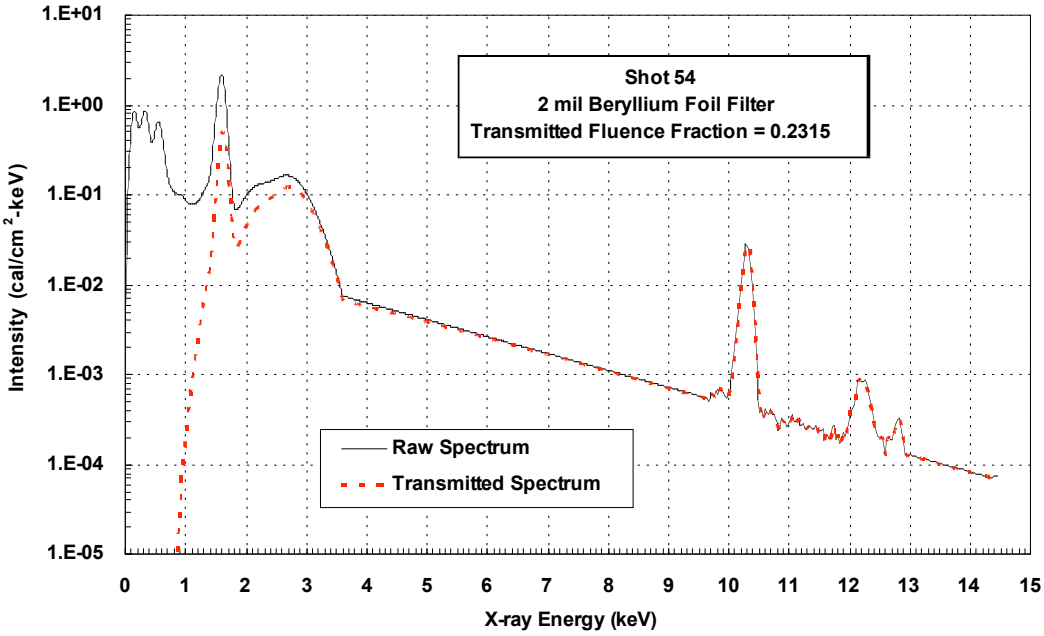

Figure C-3. Raw and Transmitted Spectra – Shot 54

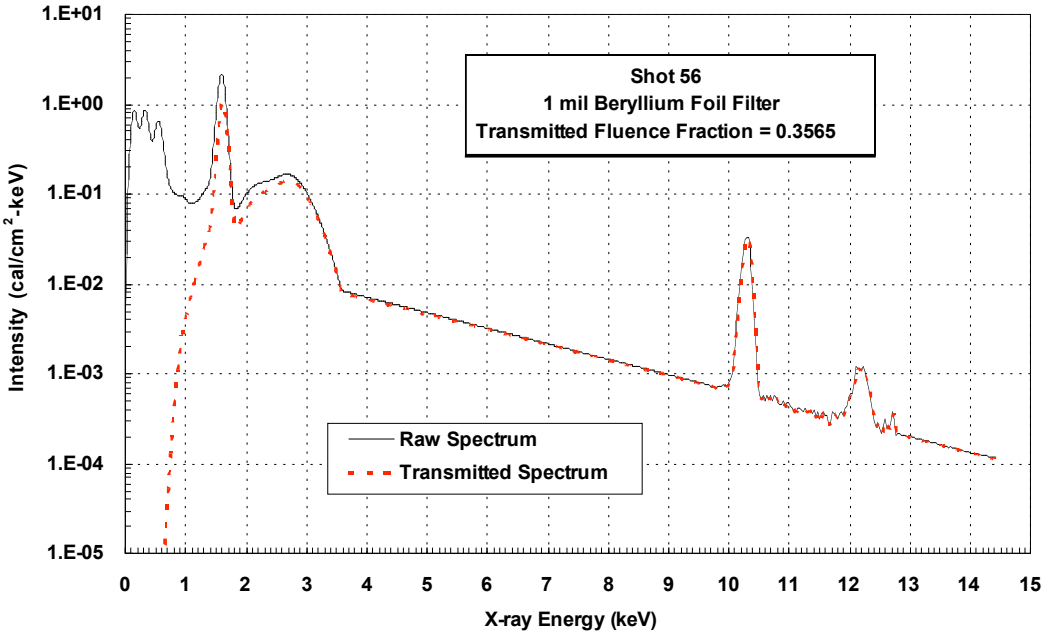

Figure C-4. Raw and Transmitted Spectra – Shot 56

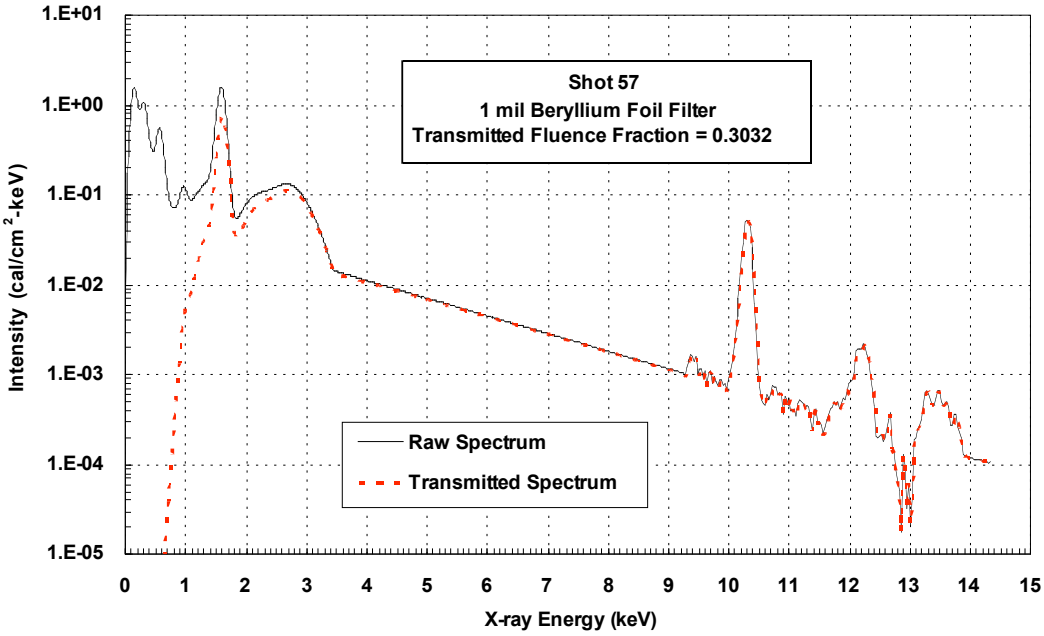

Figure C-5. Raw and Transmitted Spectra – Shot 57

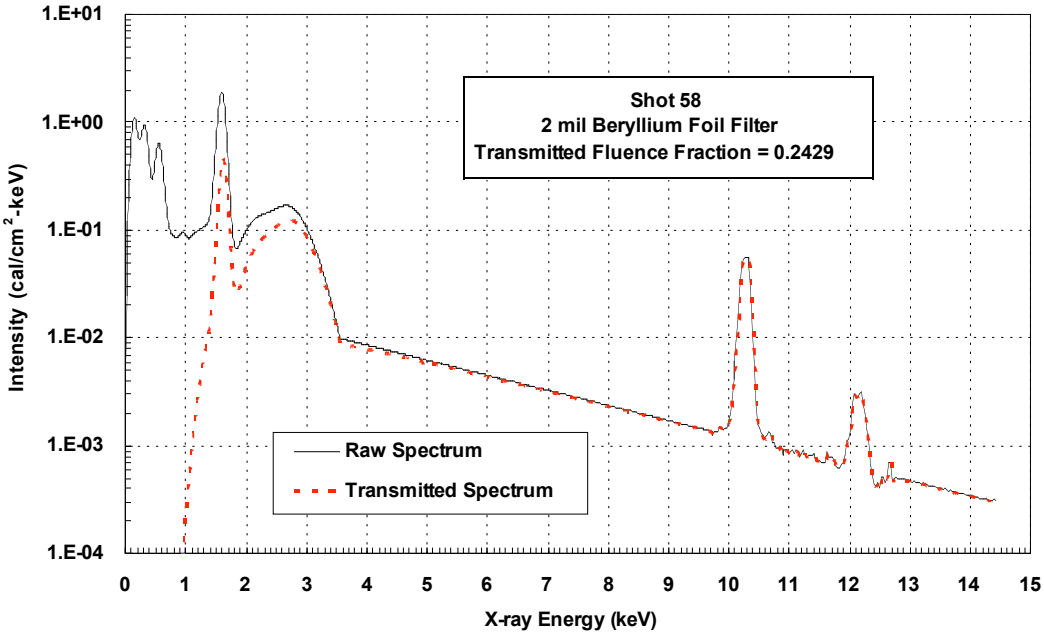

Figure C-6. Raw and Transmitted Spectra – Shot 58

Appendix D

Initial Peak Temperature Profiles

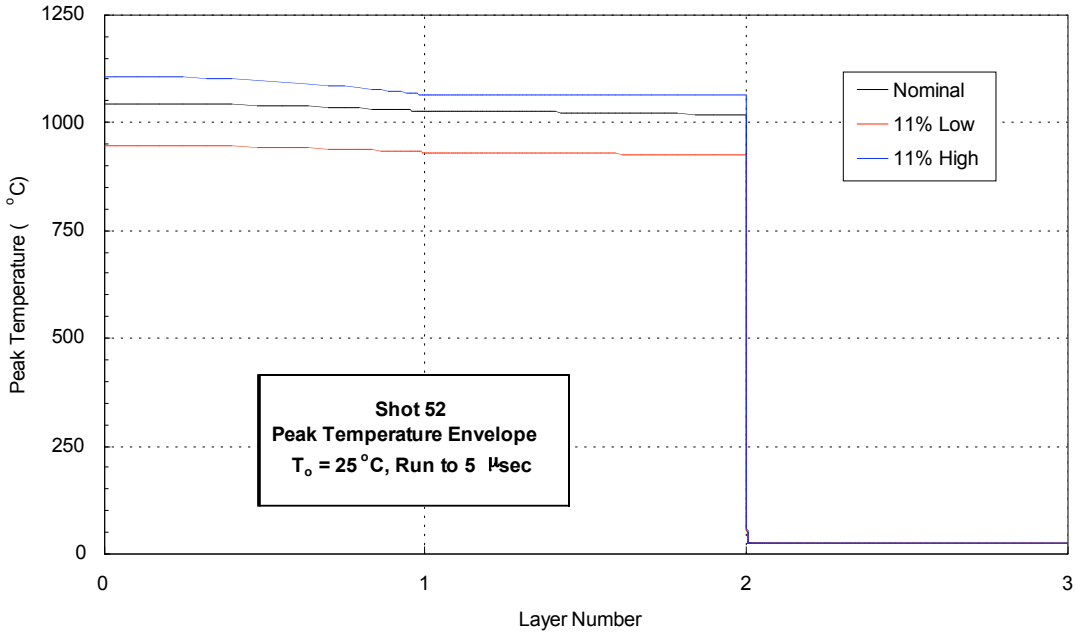

Figure D-1. Peak Temperature Profiles for Shot 52

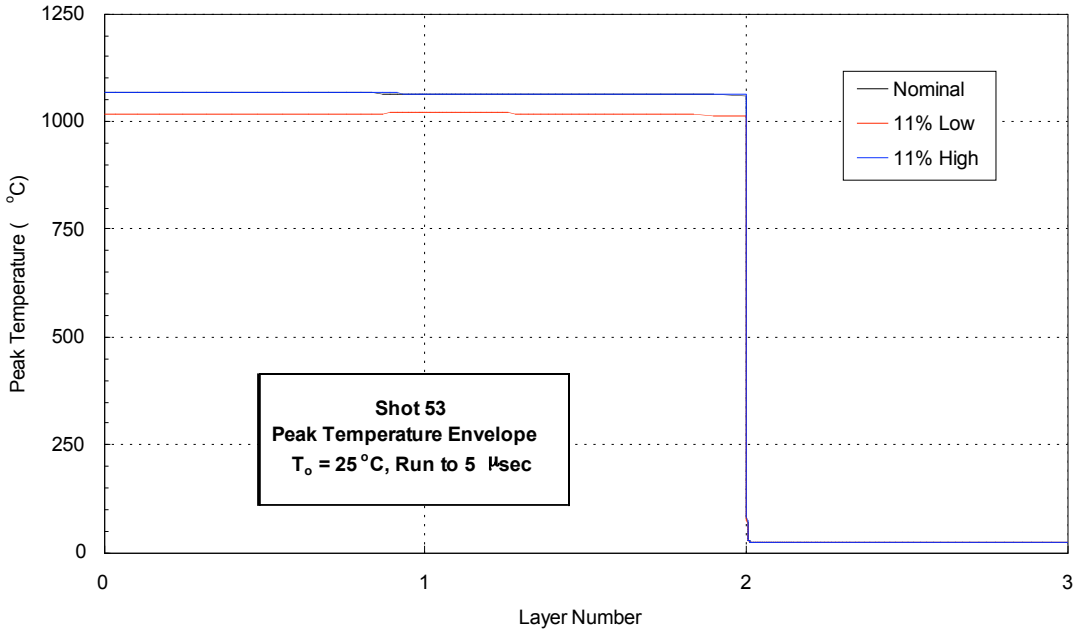

Figure D-2. Peak Temperature Profiles for Shot 53

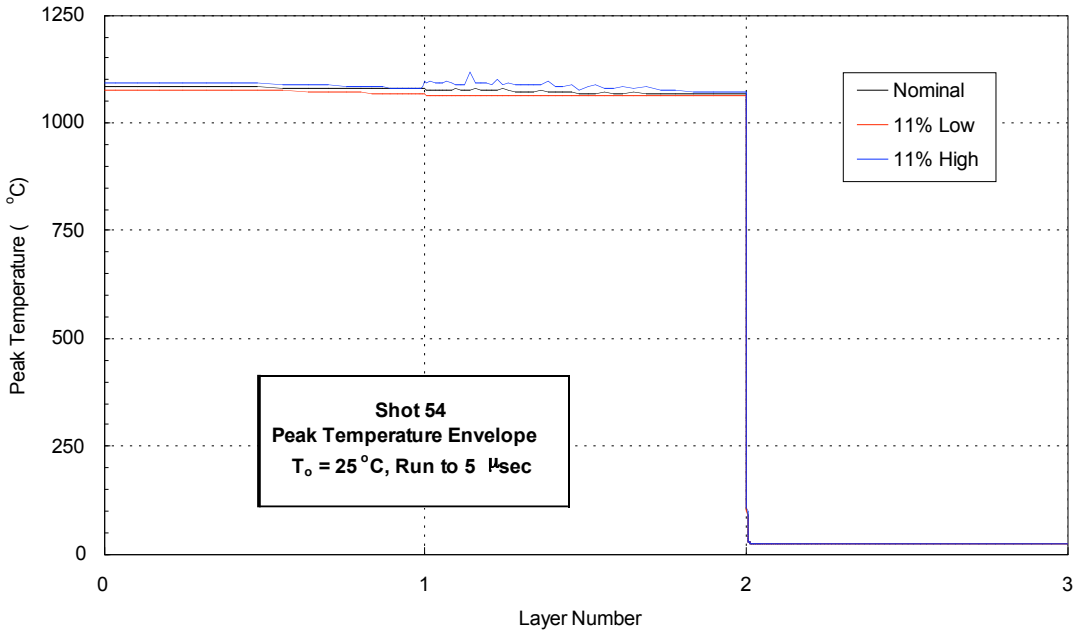

Figure D-3. Peak Temperature Profiles for Shot 54

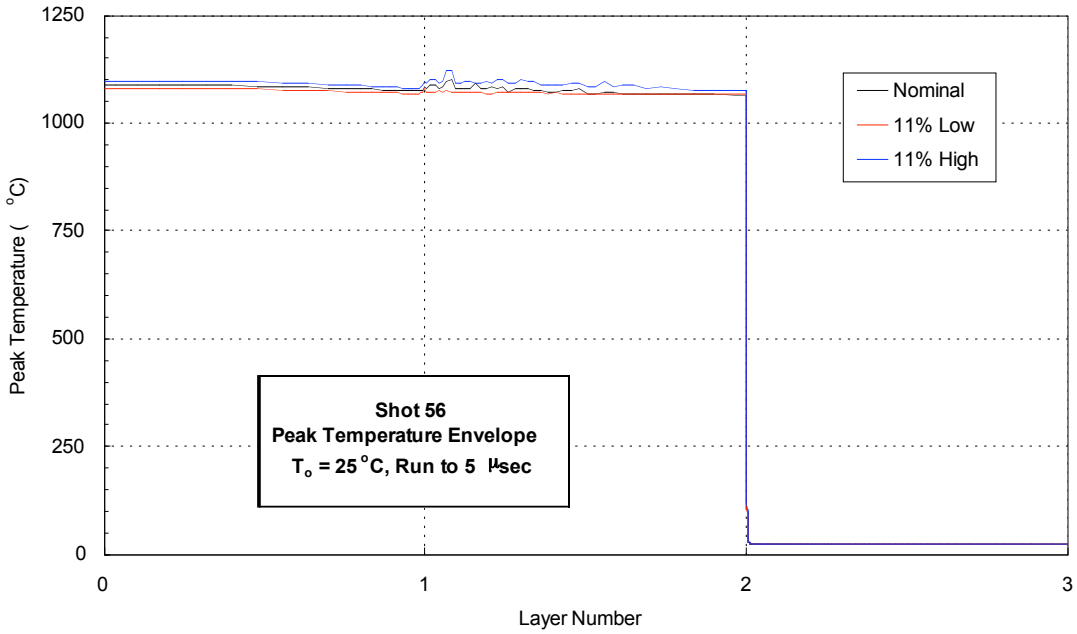

Figure D-4. Peak Temperature Profiles for Shot 56

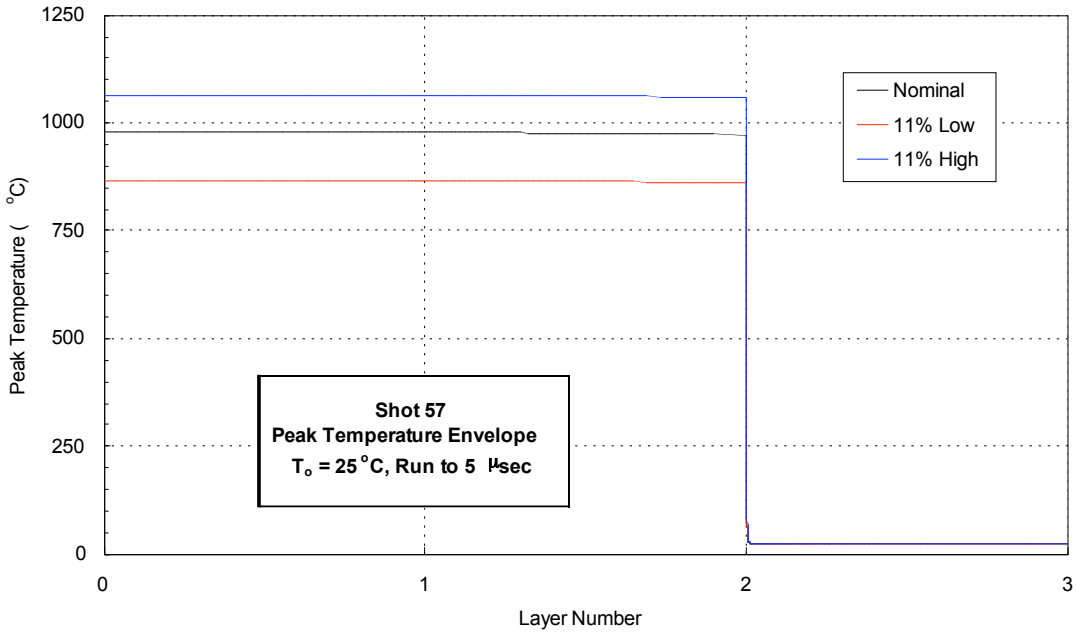

Figure D- 5. Peak Temperature Profiles for Shot 57

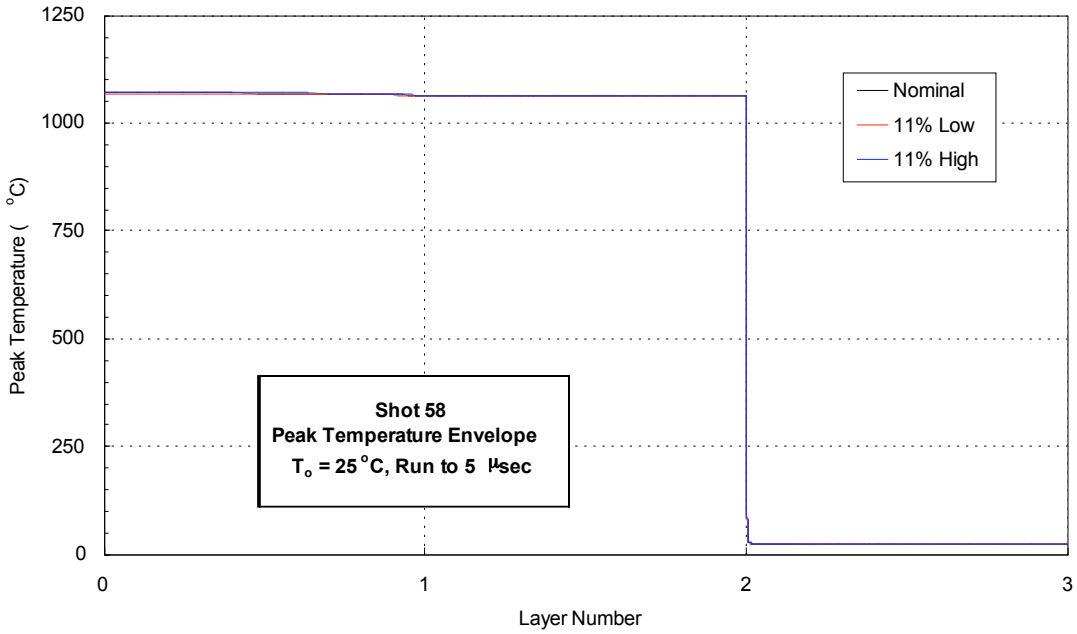

Figure D-6. Peak Temperature Profiles for Shot 58